

Technische Universität Ilmenau
Fakultät für Maschinenbau
Fachgebiet Fertigungstechnik



Development of Friction Stir Processing of CNT-reinforced aluminum alloy composites

MASTERARBEIT

Vorgelegt von

Anna Regensburg (B. Sc.)

Matrikelnummer

42173

Matrikel

2011

Ausgegeben am

22. Oktober 2012

Fertig gestellt zum

26. Februar 2012

Verantwortlicher Hochschullehrer

Prof. Dr.-Ing. habil. Jean Pierre Bergmann

Betreut von

Prof. Dr.-Ing. habil. Jean Pierre Bergmann

Dr. Francisco Rumiche

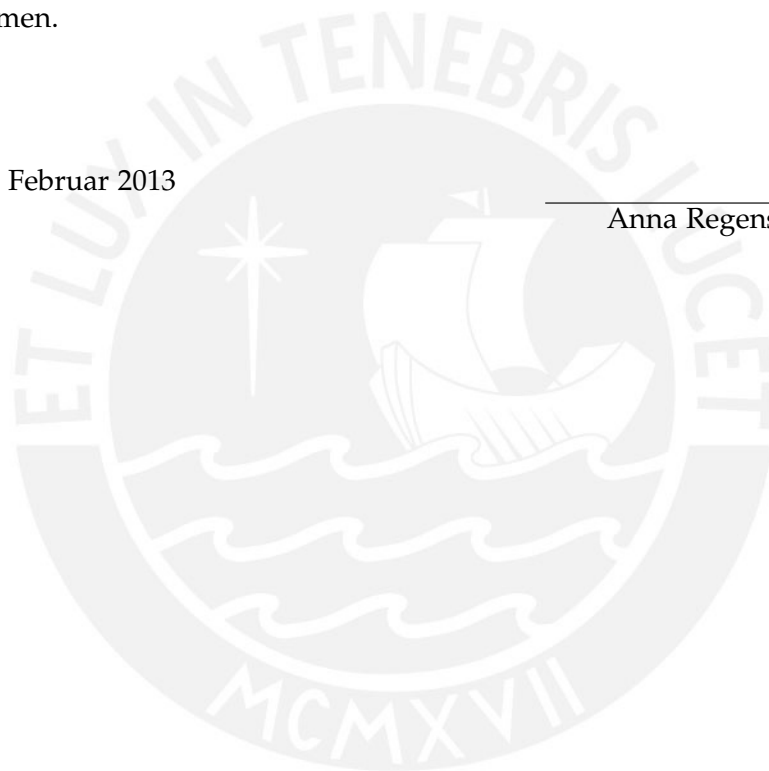
Ilmenau 2012

Selbstständigkeitserklärung

Ich versichere hiermit, dass ich die vorliegende Arbeit selbständig und ohne Benutzung anderer als der angegebenen Hilfsmittel angefertigt habe. Alle Stellen, die wörtlich oder sinngemäß aus veröffentlichten und nicht veröffentlichten Schriften anderer entnommen sind, sind als solche kenntlich gemacht. Die Arbeit ist in gleicher oder ähnlicher Form noch nicht als Prüfungsarbeit eingereicht worden. Ich habe die Hinweise für das Anfertigen wissenschaftlicher Arbeiten zur Kenntnis genommen.

Ilmenau, den 28. Februar 2013

Anna Regensburg (B. Sc.)



Kurzfassung

Carbon Nanotubes (CNTs) bieten durch ihre Vielzahl an herausragenden Eigenschaften, wie beispielsweise Wärmeleitfähigkeitswerten von über $3000 \text{ W}/(\text{m K})$ und Festigkeiten im Bereich von 100 GPa , hervorragende Voraussetzungen für die Anwendung in Verbundwerkstoffen.

Für die praktische Anwendung als Verstärkung in Metal Matrix Composites (MMCs) stellt sich vor allem die Herausforderung, die gewünschten Eigenschaften mit minimalen Verlusten vom Nano- in den Makrobereich zu übertragen. Die bisher dafür genutzten Verfahren der Pulvermetallurgie zeigen bereits vielversprechende Ergebnisse, führen allerdings zu langen Prozesszeiten sowie Beschädigung der CNTs bei langen Mahlzeiten während des Mischens mit dem Metallpulver.

Die Nutzung des Rührreibschweißens zur Herstellung CNT-verstärkter MMCs bietet an dieser Stelle eine Reduzierung der Prozesszeiten sowie die Umsetzung des Fertigungsprinzips "Funktionswerkstoff an Funktionsstelle". Hierbei wird der Grundwerkstoff durch die Bearbeitung mit einem speziell ausgelegten Werkzeug durch Reibungswärme plastifiziert und das CNT-Pulver dabei in die oberflächennahen Bereiche des Matrixmaterials „eingerührt“.

Bisherige Untersuchungen zu diesem Thema heben immer wieder die gleichmäßige Verteilung der CNTs im Grundwerkstoff als Hauptherausforderung hervor. Lösungsansatz hierfür ist bisher der Einsatz des Multipass-FSP, bei dem das Werkzeug zwei- bis fünfmal über die Schweißnaht fährt und das CNT-Pulver somit gleichmäßig verteilt. Das führt in der Regel jedoch zur Beschädigung beziehungsweise vollständigen Zerstörung der röhrenförmigen Struktur der CNTs. Da eine auffällige Gemeinsamkeit bisheriger Untersuchungen in der Nutzung konventioneller Werkzeugprofile mit zylindrischem Stift oder Gewindestift besteht, wurde in der vorliegenden Arbeit das Prozessverhalten verschiedener Werkzeugprofile analysiert, welche laut Literatur ein besseres Mischverhalten aufweisen. Dafür wurden CNT-gefüllte Kanäle in einer Al 5086-Platte unter Variierung der Einflussgrößen mit den verschiedenen Werkzeugprofilen bearbeitet und die Proben anschließend durch Metallographie, Härte- sowie Widerstandsmessung und REM-Untersuchungen ausgewertet. Letztendlich wurde durch Einsatz eines dreieckigen Profils die Vermeidung von Hohlräumen in der Schweißnaht sowie eine gleichmäßige, oberflächennahe Verteilung der CNTs erreicht.

Abstract

Owing their wide range of exceptional properties, for example thermal conductivity values of more than 3000 W/(m K) and strength in the range of 100 GPa, Carbon Nanotubes (CNTs) have recently gained much attention as reinforcement for composite materials.

Considering the practical application in metal matrix composites (MMCs), transferring those favourable properties from nano to macro scale represents a main challenge. Methods of the powder metallurgy route show promising results so far, but also lead to long process times and damage of the tubular structure of the CNTs due to prolonged ball milling times.

At this point, the application of Friction Stir Processing (FSP) for fabricating CNT-reinforced MMCs offers the possibility to reduce process times and realize the required reinforcement at the relevant location of the component. The process uses a specially designed tool with a pin to plasticize the base material by frictional heating and thus incorporate the reinforcing material by stirring it into the workpiece.

Investigations, that have been carried out on this subject, generally consider the uniform dispersion of the CNTs within the matrix as the key challenge of this process. So far, the solution herefore is the application of multipass-FSP in order to distribute the CNTs uniformly by processing the weld up to five times with alternating welding direction. This method usually leads to damage or even destruction of the tubular structure of the CNTs. Regarding all investigations on this subject, it can be noticed, that only conventional tool profiles like cylindrical or threaded were used for the experiments, though other profiles like square or more complex ones are considered to exhibit an increased mixing effect. Therefore the objective of the thesis is to analyse the performance of four different tool geometries under varying parameters and their influence on the CNT dispersion and general MMC composite properties. Channels were cut into an Al 5086 plate, filled with CNT-powder and processed by the different tools. The results were evaluated by metallographic analysis, hardness and electrical resistance measurement and SEM analysis. Among the different geometries, the triangular profile produced defect-free welds over the whole parameter set and distributed the CNTs uniformly along a wide area close to the weld surface.

Contents

1	Motivation	1
2	State of technology	3
2.1	Friction Stir Processing	3
2.1.1	General	3
2.1.2	Material science mechanisms	6
2.1.2.1	Strain hardening	6
2.1.2.2	Recrystallisation	6
2.1.3	Tool geometry	8
2.1.3.1	Shoulder geometry	9
2.1.3.2	Pin geometry	10
2.1.4	Processing Parameters	14
2.1.5	Material flow	15
2.1.5.1	General	15
2.1.5.2	Tracer technique	15
2.1.5.3	Simulation	17
2.1.5.4	Influence of the tool geometry	20
2.1.6	Defect characterization	24
2.2	Carbon Nanotubes	25
2.2.1	Structure and properties	25
2.2.2	Application in Metal Matrix Composites	26
2.3	Synthesis of CNT-Aluminum composites by FSP	29
3	Objective	33
4	Experimental Procedure	34
4.1	Base materials	34
4.2	Sample preparation	34
4.3	Processing	36
4.4	Sample characterisation	37
5	Results	39
5.1	Plan views	39

5.2	Metallography	40
5.2.1	Cylindrical profile	41
5.2.2	Triangular profile	43
5.2.3	Square profile	45
5.2.4	Fluted profile	46
5.3	Flow arm and nugget size	48
5.4	Mircohardness measurements	49
5.5	Electrical resistance	50
5.6	SEM analysis	51
5.7	Tool wear	53
5.8	Summary	53
6	Discussion	56
6.1	Material flow	56
6.2	Heat flow	57
6.3	Electrical resistance	58
6.4	Error consideration	59
6.4.1	Process	59
6.4.2	Sample preparation	59
7	Summary	60
8	Outlook	61
	Appendix	LXIII
	List of tables	LXXIII
	List of figures	LXXVI
	Bibliography	LXXVII

1 Motivation

The steady increasing need for lightweight, but strong components in various areas like the automotive and energy industry shows the limits of conventionally applied materials. While higher stiffness and strength values are required to comply with increased safety regulations and bearing loads, the weight of the component has to be kept as low as possible to enable improved payload and fuel efficiency. Therefore composite materials have gained much attention recently as material properties can be tailormade by reinforcing conventional materials with light, but high strength fibers or particles.

Discovered in 1991 by Sumio Iijima, Carbon Nanotubes (CNTs) have been subjected to various investigations since then. The reason herefore is their wide range of exceptional properties. Consisting of one or more graphite sheets wrapped into a cylindrical tube, the one-dimensional structure of the CNTs allows them to carry high currents up to $4 \cdot 10^9$ A/cm² over long distances, practically without heating. Thermal conductivity also reaches exceptional values up to 6000 W/(m K) on single CNTs, thus exceeding the values of natural diamond and the basal plane of graphite. At the same time, they show a very low coefficient of thermal expansion (CTE \approx 0), which makes them very suitable for thermal management applications. Apart from that, their mechanical properties even exceed those of carbon fibers. Stiffness values up to 1000 GPa and strength in the range of 100 GPa combined with an extremely low density make them the strongest fibers known to mankind.

On the other hand the extreme small diameters of 0.4 nm to 100 nm for single- and doublewalled and more for multiwalled CNTs make it difficult to transfer their outstanding properties to the macro scale without mayor losses. The most common methods for fabricating CNT-reinforced composites are powder metallurgy procedures like sintering and hot pressing. Though high increases in mechanical properties have already been achieved, the uniform distribution of the CNTs within the metal matrix still represents a key challenge. Due to their high specific surface, agglomeration can hardly be avoided. Ball milling with long milling times is used to provide a homogeneous mixture of metal and CNT powder, but rather leads to damage or even destruction of the tubular structure of the CNTs.

At nearly the same time, when CNTs were discovered, the joining technique Friction Stir Welding (FSW) was invented by The Welding Institute (TWI) of Cambridge. This process allows to join abutting plates without melting the base material. Therefore a specially designed tool with a pin is required. During the process it is plunged into the workpiece surface and by the tool movement and the resultant frictional heating, the material is softened and plasticized.

Thus the joint is produced in solid state and without requiring consumables like wires or shielding gas. The same principle was applied on monolithic workpieces in 2001 and called Friction Stir Processing (FSP). Using this method, composites can be produced by practically stirring the reinforcing material into the workpiece.

CNTs have already been incorporated into aluminum alloy surfaces. Investigations show, that the tubular structure survives the high process forces during FSP and that the reinforcement leads to a strong increase in hardness and tensile strength. In spite of this fact, a uniform distribution of the CNTs within the metal matrix has yet to be demonstrated. Especially for heat sink or electrical applications CNTs exhibit promising properties but this requires an excellent distribution and interfacial bonding within the composite.



2 State of technology

2.1 Friction Stir Processing

2.1.1 General

In 1991 the joining technique Friction Stir Welding (FSW) was invented by The Welding Institute (TWI) of Cambridge. Using a specially designed tool with a pin, two abutting plates are joined without melting the base material. The transversal and rotational movement of the tool causes severe plastic material deformation and localized heating due to friction between the tool and the workpiece. The heating furthermore softens the material and therefore allows a material movement from the front to the back of the pin. Thus the plates are joined in solid state as shown in figure 2.1 (See Mishra et al. [MM05]).

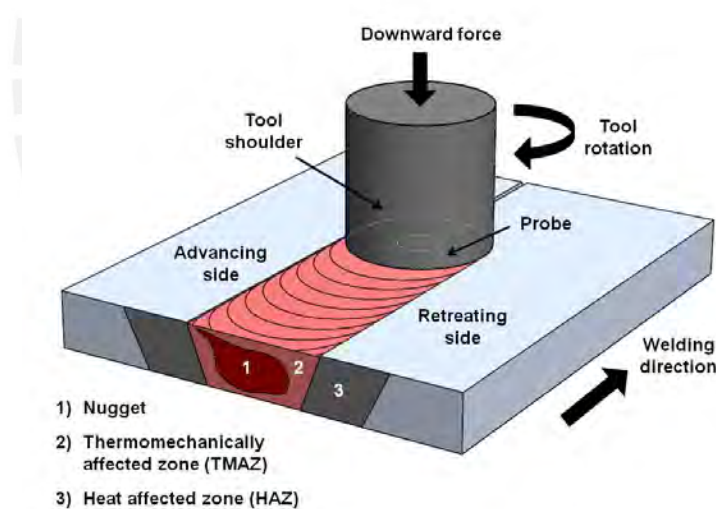


Figure 2.1: Schematic drawing of friction stir welding

Figure 2.1 also shows the different areas formed in the postweld microstructure. Threadgrill [PT97] defined them as following, as one of the first classifications they have widely been used since then (See Mishra et al. [MM07]):

- *Unaffected material or parent metal*: The material was not affected by deformation or heat, so that no changes in microstructure or mechanical properties occurred, but it could have experienced a thermal cycle from the weld.

- *Heat-affected zone*: The material was not affected by deformation but the closer distance to the weld-center led to changes in the microstructure and/or mechanical properties due to heat exposure.
- *Thermomechanically affected zone (TMAZ)*: In this area the material was plastically deformed by the FSW/FSP tool and also affected by the friction induced heat. Thus changes in the microstructure and/or mechanical properties occurred. Generally this area shows a distinct boundary to the nugget.
- *Weld nugget*: This area is fully recrystallized as it was occupied by the tool pin. For FSP the term *stir zone* also refers to this area. Due to the complex material flow, the microstructure of the weld nugget usually is not homogeneous.

As shown in figure 2.1, an asymmetrical nugget is produced, when conventional tools are used. This is caused by the superposition of the rotation and forward movement of the tool along the welding direction. At one side of the weld the tool rotation direction (at the outer edge of the weld) is parallel to the tool travel direction and this side is called "advancing side". At the other side these directions are opposite to each other, which therefore is named "retreating side".

The plastic deformation at elevated temperature results in an enhanced microstructure, so that good mechanical properties can be achieved in the weld. Based on the principles of friction stir welding, Mishra et. al [MM01] developed friction stir processing (FSP) to apply the concept on monolithic workpieces as shown in figure 2.2.

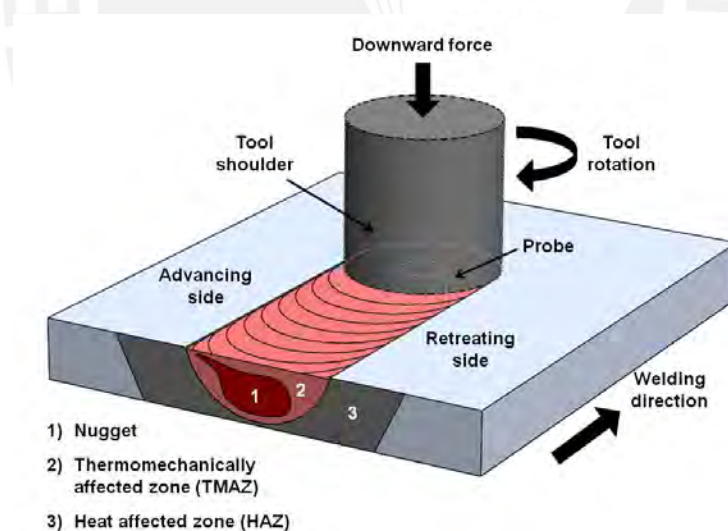


Figure 2.2: Schematic drawing of friction stir processing

Regarding the main classification of manufacturing processes according to DIN 8580, FSW can be assigned to Friction Welding, which is a subgroup of welding with pressure as shown in figure 2.3. For this case, FSP is also assigned to this group, as a composite is produced out of bulk metal and formless powder.

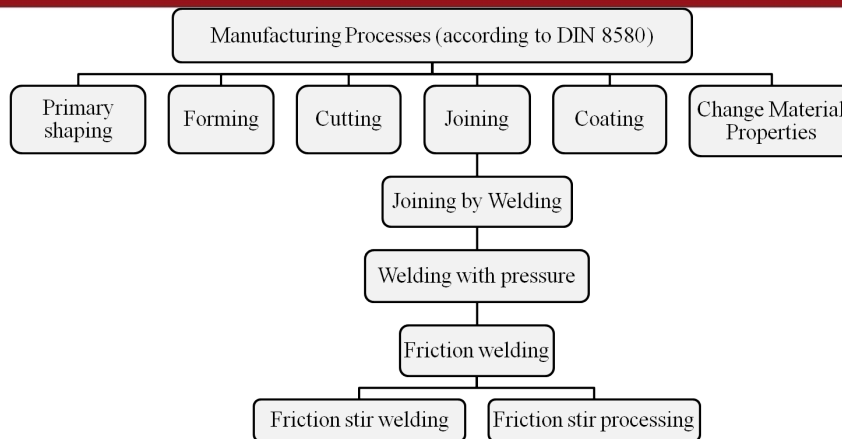


Figure 2.3: Classification of manufacturing processes according to DIN 8580

The combination of friction induced heating and intense deformation causes dynamic recrystallisation in the stirred zone (SZ). At first, strain hardening occurs as the grain boundaries inhibit the movement of dislocations. Exceeding the critical degree of deformation and about 50% of the melting temperature, recrystallisation occurs and new grains are formed. In alloyed metals, dissolved alloy atoms produce two effects. First they avoid softening by inhibiting dislocation movement, second they also slow down grain growth, which normally occurs right after grain formation. Thus a fine-grained microstructure is achieved, as shown in figure 2.4.

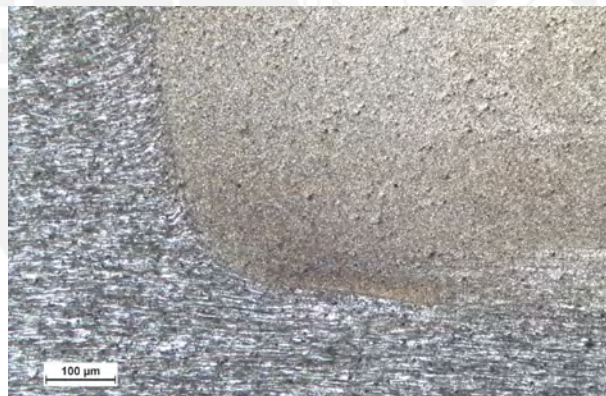


Figure 2.4: Typical, fine-grained microstructure at the limit of TMAZ (left) and nugget (right)

Investigation have shown, that the "FSP parameters, tool geometry, material chemistry, work-piece temperature, vertical pressure, and active cooling" affect the grain size significantly [Ma08]. Thus mechanical properties can be tailormade by varying certain parameters. The microhardness for example increases with decreased grain size. Furthermore the occurrence of superplasticity can be achieved at higher strain rates or lower temperatures.

There is also the possibility to produce metal matrix composites (MMCs) by incorporating particles into the surface, using the mixing effect of the tool. Hence surface composites with enhanced mechanical properties and uniform particle distribution can be fabricated to reinforce

components locally. FSP has recently been subject to several investigations, regarding various components and effects of the process. Due to the complex material flow and several other factors interacting and influencing the results, the knowledge is still restricted and tools are commonly designed on an intuitive and experimental basis.

2.1.2 Material science mechanisms

2.1.2.1 Strain hardening

Strain hardening occurs in metals, which are subjected to plastic deformation. During the deformation dislocations glide through the material. As shown in figure 2.5, these gliding movements are restrained by grain boundaries or other barriers, where the dislocations are stagnating. Thus further gliding is avoided and the required shear stress is increased respectively.

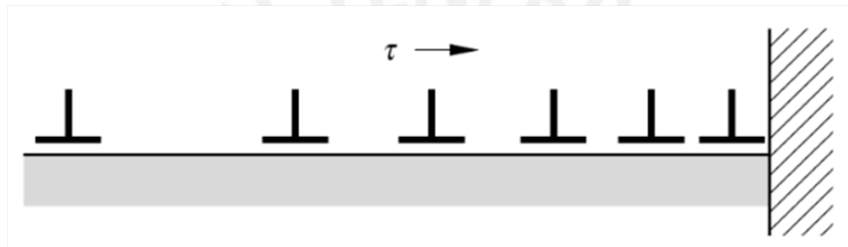


Figure 2.5: Holdup of dislocations at a barrier [BCHS03]

Regarding polycrystalline metals the gliding of the dislocations is mainly restrained by grain boundaries due to their high energy content. At the same time these and other barriers like dislocation lines and inclusions within the microstructure provide sources for new dislocations. The interaction between the dislocations therefore leads to the following effects (See Schulze et al. [SHBK08]):

- steady stress increase required for further deformation,
- increasing resistance to plastic deformation,
- increase of yield and tensile strength,
- increase of hardness.

2.1.2.2 Recrystallisation

Due to the intense plastic deformation during FSP, the material is subjected to strain hardening as mentioned before. The locations, where the dislocation gliding gets restrained, show high density of defects and an increased lattice strain. Crystallisation nuclei are formed and trigger recrystallisation processes at a certain temperature increase. According to Schulze

et. al [SHBK08] the following changes in microstructure and material properties can occur at increased temperatures:

- increase of vacancy concentration,
- facilitating of diffusion processes,
- formation of new gliding systems due to climbing and cross sliding of dislocations,
- enabling of grain boundary deformation,
- increasingly simplified deformation,
- stability of the microstructure decreases,
- recrystallization of cold deformed material,
- aging of hardened material,
- workpiece surface reacts more easily with the environment,
- problems with corrosion and scaling.

Thermally activated processes like phase changes, crystal regeneration and recrystallisation depend on the mentioned effects. As shown in figure 2.6, the critical degree of deformation for recrystallisation has to be exceeded at increased temperature to enable the formation of new grains, starting from the crystallisation nuclei. Thus the microstructure is rebuilt to a level with less dislocations.

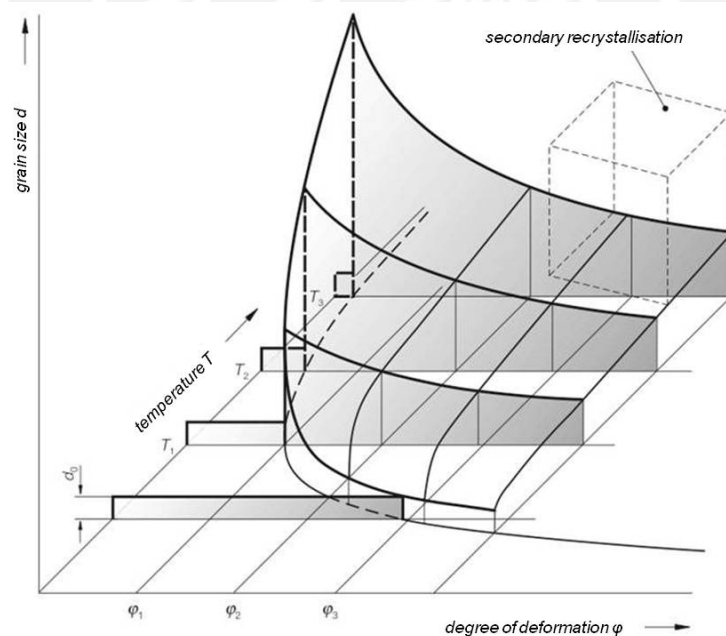


Figure 2.6: Dependence of the recrystallisation on temperature and deformation [SHBK08]

As the degree of deformation determines the number of crystallisation nuclei, the combination of low deformation and high temperature can cause excessive grain growth as shown in figure 2.6 at the degree of deformation ϕ_1 and temperature T_3 . Prolonged annealing times lead to the same result. Eventually, the excessive grain growth comes along with hardness and strength loss while the ductility increases as shown in figure 2.7.

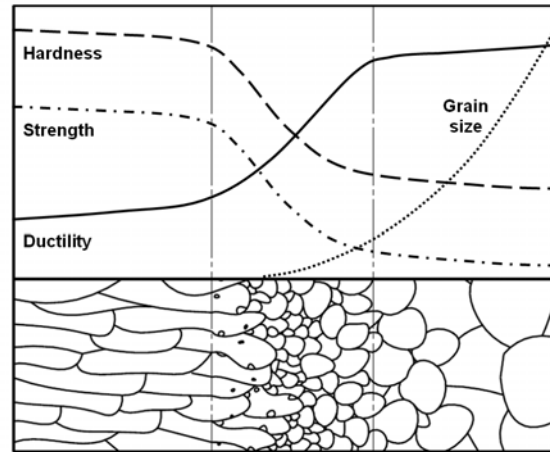


Figure 2.7: Microstructure and property change during recrystallisation

During hot forming, recrystallisation processes can occur during the actual forming, if the temperature is higher than half of the melting temperature, thus exceeding the recrystallisation temperature. This variation is called dynamic recrystallisation. When high yield stresses are applied, small grain sizes are achieved, so that the microstructure can be tailormade, using different degrees of deformation.

2.1.3 Tool geometry

The tool geometry significantly influences the process and therefore plays an important role for the result. Adapted from the FSW process, the FSP tool consists of a shoulder and a pin. The shape and size of the tools can vary and is often based on former investigations. Tools without pin are used as well. Studies on material flow, tool stress and load help to understand the complex interactions, but in general, the design is done empirically.

The main function of the FSP tool is providing localized heating and material flow. The heating is provided by the friction between the tool surface and the base material. Usually, the main part is provided by the shoulder, though the pin already provides friction when plunging into the material. The shoulder also limits the area of heating, while the pin size and shape mainly affect the flow of the plasticised material. Therefore the relative size of shoulder and pin also plays an important role (See Mishra et al. [MM05]).

Differences in the heating shares occur depend on the geometry of the workpiece. Especially when welding thick workpieces or using large plunging depths, the pin is providing the majority of the heating due to the large contact surface.

2.1.3.1 Shoulder geometry

The tool shoulder is designed to provide frictional heating at the workpiece surface and the necessary downward force. Figure 2.8 summarises some common shoulder shapes. Usually, a cylindrical outer surface is used. Due to the small plunge depth the influence of this shape is relatively small in general.

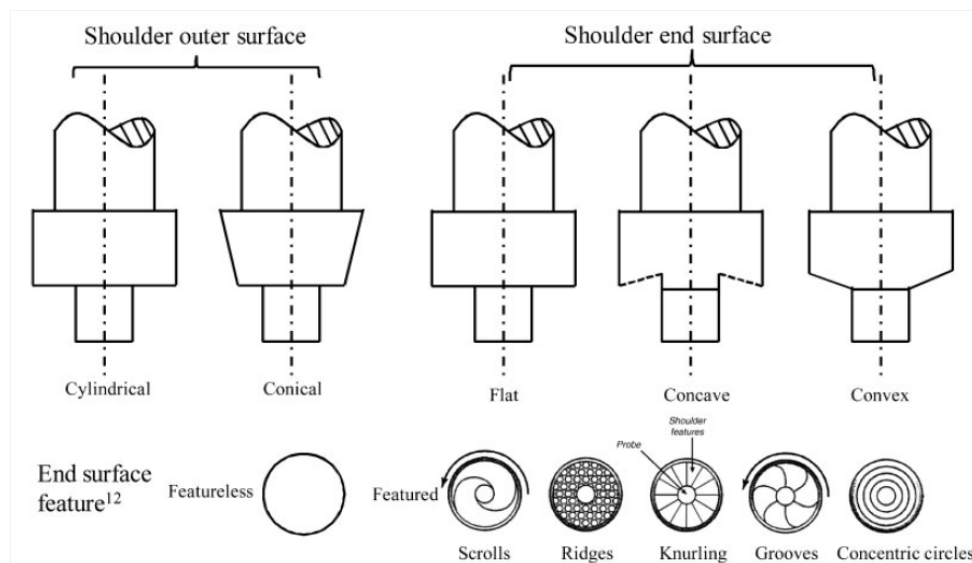


Figure 2.8: Summary of typical shoulder shapes [ZCLW12]

The shoulder end surface however can show more variations. Conventionally, a flat shoulder is used. At the same time, this is the simplest design, but not effective to avoid excessive material flash and keep the flowing material under the bottom of the shoulder (See Rai et al. [ZCLW12]). Therefore, concave shapes with a small inclination angle up to 4° are used, so that the material displaced by the pin is fed into the shoulder cavity.

Furthermore, certain features are used to enhance the material flow by increasing "material friction, shear and deformation for increased workpiece mixing and higher weld quality" [ZCLW12]. Some typical feature like scrolls and concentric circles are also shown in figure 2.8. From these features, scrolls are the most commonly used ones. A spiral channel is cut from the edge of the shoulder to the pin and enhances the material flow as it forces the plasticised material to the pin. Thus, the tool does not have to be tilted. In addition, the constant shearing of the material in the channels provides increased deformation and frictional heating.

2.1.3.2 Pin geometry

The shape of the tool pin strongly affects the flow of the plasticised material. The pin is supposed to shear the material in front of the tool and transport it to the back. Figure 2.9 summarises different types of tool shapes. Conventionally, cylindrical pins with flat bottoms are used due to easy fabrication. They also show better wear resistance regarding high strength or abrasive material, as features like threads and edges can easily be worn away. Therefore, they are usually used for FSW of plates up to 12 mm thickness. For increased stirring like needed for FSP application or thicker plates, special tool features are required. Below, a few selected tool shapes and geometry variations are introduced, focussing especially on applicability to FSP and enhanced material flow or mixing effect.

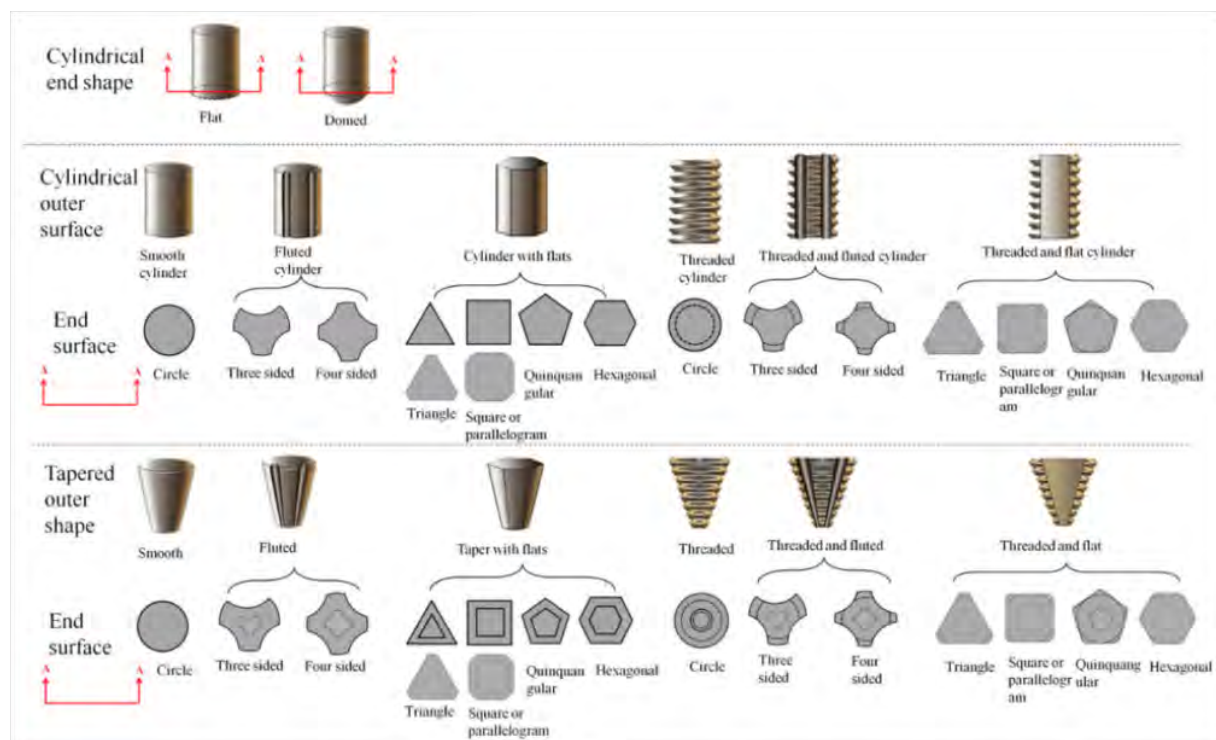


Figure 2.9: Summary of typical pin shapes [ZCLW12]

Tools with flutes like the "trifluted" tool or threads have become popular as they increase the material flow compared to cylindrical pins (See Rai et al. [RDBD10]). The enlarged contact area with the workpiece leads to increased frictional heating and deformation. Especially threads show interesting effects for FSP. Putting a left hand threaded tool under clockwise rotation provides a downward force along the thread, so that the materials circulates multiple times around the pin before it moves to the back of the tool. According to Zhang et al. [ZCLW12] stirring, void closure and oxide breakdown are promoted under these conditions. Further investigations [TNN⁺96] also showed, that the addition of flats to the tool shape enhances the material flow as these flats act like paddles or cutting edges. They cause more turbulences in

the material flow as the plasticised material is trapped at the flat and later released behind the tool, which is supposed to increase the mixing effect.

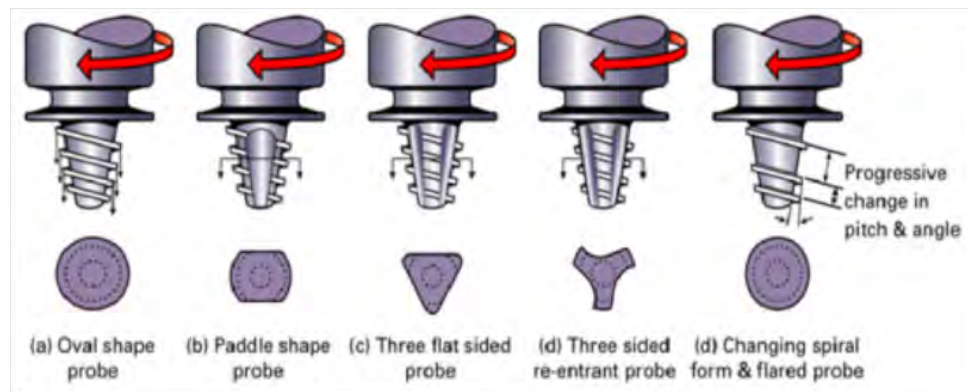


Figure 2.10: Variations of the Whorl pin geometry [MM07]

Whorl Pin

Another significant improvement in FSW/FSP tool designs is the development of the Whorl pin by TWI in 2001 [TNS01]. Using a conical pin with a helical ridge on its surface, the displaced volume could be reduced by 60% compared to a cylindrical pin with the same diameter. Hence, higher travel speeds could be realized without producing voids, as the helical ridge shows effects like an auger, causing a significant downward force. Figure 2.10 shows some variations in the design of this tool.

MX Triflute Pin

Based on this principle, Thomas et al. [TNS01] refined the design of the Whorl pin by cutting three flutes into the helical ridge as shown in figure 2.11. Thus, a reduction of the displaced volume of 70% compared to cylindrical pins could be obtained. Investigations on FSW using this tool shape reported, that thick section copper and aluminum alloys have been welded successfully and that for some applications, a travel speed more than two times higher than with the previous design could be realized (See Mishra et al. [MM07]).

In summary the design features of both Whorl and MX Triflute "were reported to reduce the welding forces, enable easier flow of the plasticised material, facilitate the downward material flow and increase the interface area between the probe and the plasticised materials in order to increase heat generation" [ZCLW12].

Trivex Pin

Regarding the reduction of traverse forces, two-dimensional (2-D) computational fluid dynamics simulations were carried out to examine material flow properties around different tool geome-

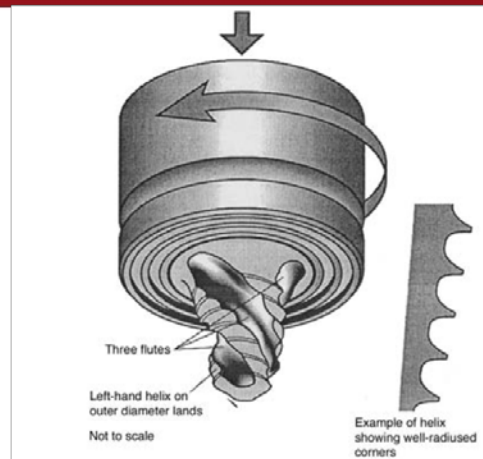


Figure 2.11: Schematic illustration of the MX Triflute pin [MM07]

tries. As a result, the featureless Trivex pin and the threaded MX-Trivex pin were developed by TWI as shown in figure 2.12 (See Mishra et al. [MM07]).

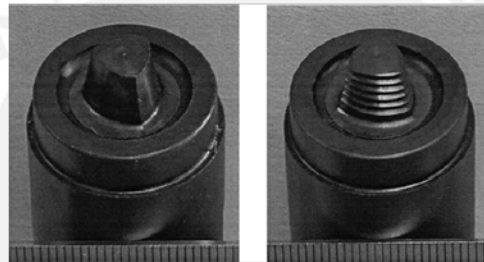


Figure 2.12: Trivex (left) and MX Trivex pins (right) [TSNF03]

Flared-Triflute and A-Skew Pin

As conventional tools like a cylindrical threaded probe lead to increased thinning of the top sheet when applied for lap welding, two new probe geometries have recently been developed by Thomas et al. [TJW03]. The bottom of the Flare-Triflute pin is flared out as shown in figure 2.13, therefore increasing swept and static volumes and changing the flow patterns around the bottom of the pin.

A-Skew tools differ from conventional tool designs in that the pin shows a slight inclination (skew) towards the tool/spindle axis as shown in figure 2.14. Due to the orbital tool motion, this design results in a weld nugget bigger than the pin. Furthermore, the increased deformation at the bottom of the pin can avoid root defects. According to Zhang et al. [ZCLW12], both tools are reported to:

- increase the swept rates and thereby increase the flow path around and underneath the probe,

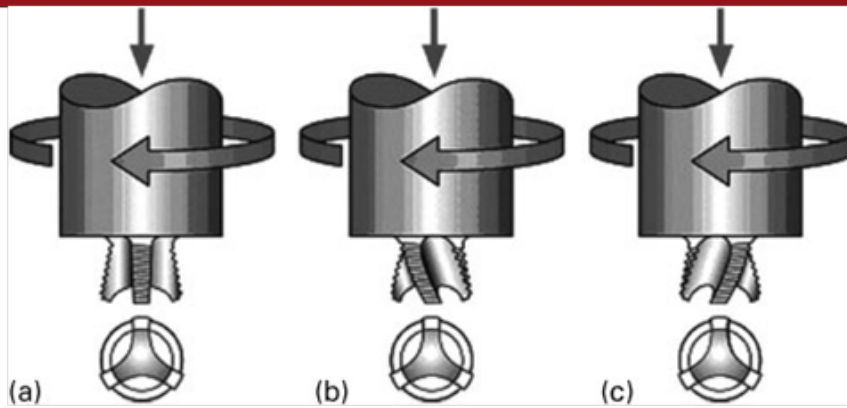


Figure 2.13: Flared-Triflute tools: (a) neutral, (b) left and (c) right hand flutes [TJW03]

- widen the welding region due to the flared-out flute lands in the Flared-Triflute and the skew action in the A-skew probes,
- improve the mixing action and favour the oxide fragmentation and dispersal at the weld interface,
- provide an orbital forging action at the weld root due to the skewed action and hence improve weld quality in this region.

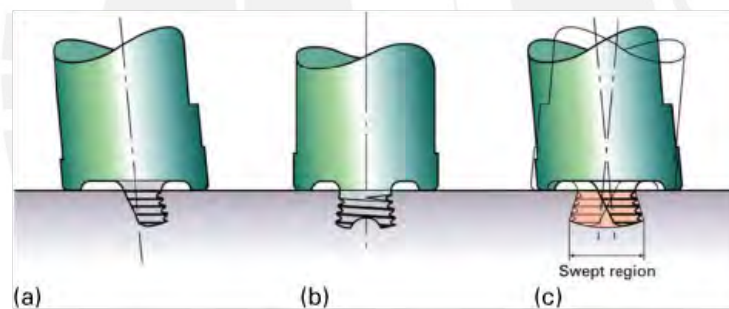


Figure 2.14: A-Skew tools: (a) side view, (b) front view and (c) swept region encompassed by skew action [TJW03]

Re-Stir Tool

The Re-Stir tool represents another variant of the skew tools. The design provides an alternation of the tool rotation "either by angular reciprocation (direction reversal during one revolution) or rotary reversal (direction reversal every one or more revolutions)" [Tho03]. This leads to a constant change of the location of retreating and advancing side as shown in figure 2.15. Hence a symmetric weld is produced and issues like a lack of deformation on the retreating side are eliminated.

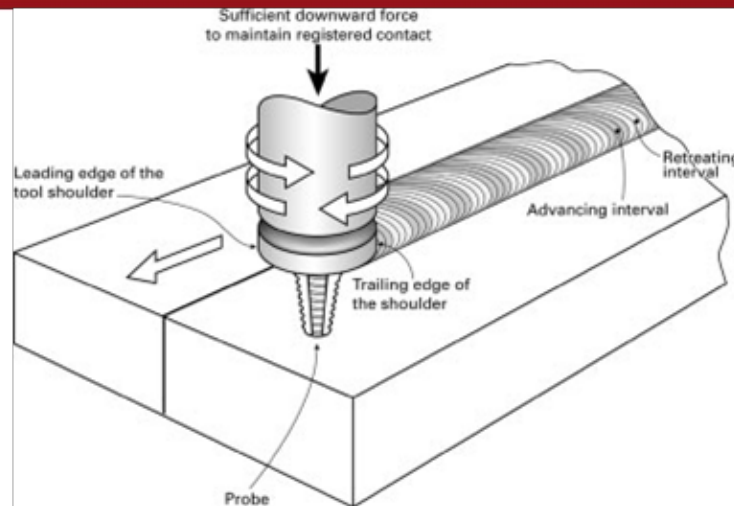


Figure 2.15: Basic principle of Re-stir [TJW03]

2.1.4 Processing Parameters

Two processing parameters significantly influence the FSP process. The tool rotation rate (ω, rpm) in clockwise or counterclockwise direction affects the stirring and mixing around the tool pin. A higher rotation rate increases frictional heating of the workpiece and thus results in higher temperature. The translation of the tool provides the movement of the plasticised material from the front to the back of the pin.

Furthermore some tool designs require a tilt of the spindle towards the processing direction to keep the stirred material under the tool shoulder, avoid excessive flash and provide an efficient material movement to the back of the pin. The insertion depth of the pin also is an important parameter, which usually depends on the pin height. Inserting the pin too little leads to the forming of channels or surface grooves as the shoulder does not get in contact with the surface to move the material efficiently. On the other hand a deep insertion of the shoulder produces excessive flash and therefore thins the plate (See Mishra et al. [MM07]). To keep shoulder and workpiece surface in contact, a sufficient down force is required, so that a uniform joint is produced even under tolerance errors.

For some FSW/FSP processes, external heating or preheating is important. When materials with high melting points or high thermal conductivity are used, the friction induced heat might not be sufficient to soften and plasticize the material around the tool. Therefore external heat sources can be used to enhance the material flow. For other cases cooling can be applied as well to avoid excessive grain growth in materials with lower melting point (See Mishra et al. [MM07]).

2.1.5 Material flow

2.1.5.1 General

The material flow of FSW/FSP processes is very complex as it strongly depends on tool geometry, process parameters and material. These factors also control the volume of heated and plasticised material. Especially the tool geometry has a significant influence, so that general theories can hardly be set up.

Figure 2.16 shows the cross section of a typical friction stir weld, where the weld nugget borders to the thermomechanically and heat affected zone. The size of the nugget depends on the amount of generated heat, as investigations show, that colder welds also show smaller nuggets (See Mishra et al. [MM07]).

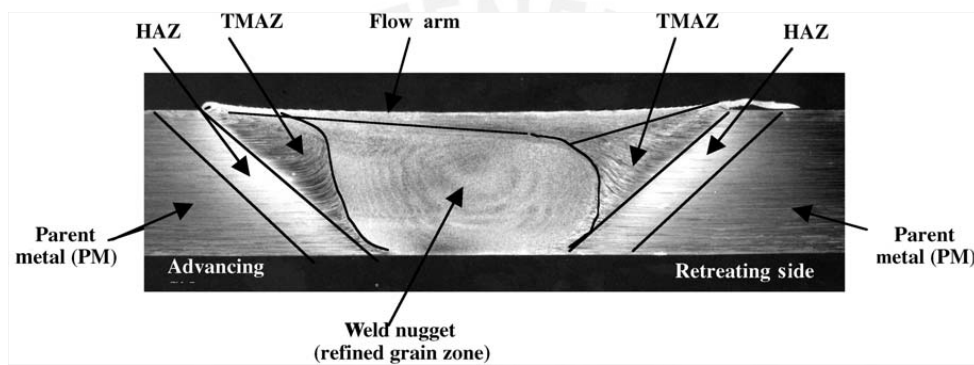


Figure 2.16: Transverse section of a friction stir weld showing different regions of the weld [MM07]

2.1.5.2 Tracer technique

One method to analyse the metal flow is the use of tracer particles, which are different to the base material and therefore track the way of the material through the process. Colligan [Col99] obtained the first definition of the flow paths during FSW by using small steel balls (0.38 mm in diameter), which were embedded at different positions along the weld. Therefore a groove was cut along the butting edge of the aluminum alloy plates and filled with the steel balls. After that the weld was run and stopped at one point along the joint without lifting the tool. A radiographic examination was performed to reveal the distribution of the tracer material compared to its original position. The results showed, that a lot of the material was simply extruded from the front to the back of the pin by passing it on the retreating side. The final position in the weld of these steel balls was also found to be higher than the original one. The rest of the material was actually stirred, it was forced down by the thread and deposited in the weld nugget. Due to the different material and geometrical properties of tracer and workpiece material, it is likely that the steel balls did not accurately reflect the material flow of

the plasticised aluminum alloy, especially regarding the material movement close to the thread (See Colligan [Col99]).

Further investigations (summarised by [MM05], Ref. 28-30) embedded the tracer material in a similar way into the path of the welding tool. Figure 2.17 shows how the tracer particles were embedded into inserts of different depths. After welding, slices of (0.25 mm were milled off the weld surface and metallographic examination was performed successively.

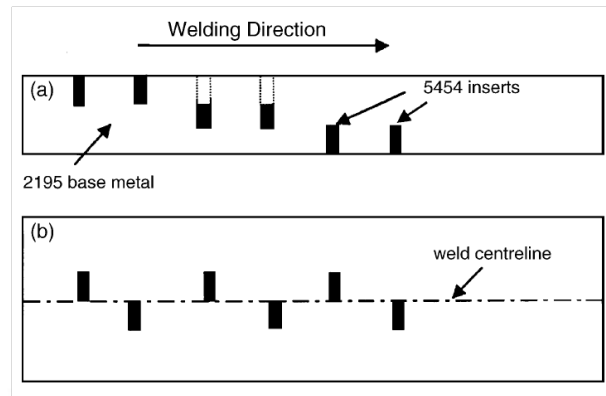


Figure 2.17: Positions of the marker inserts along the weld [MM05]

The results revealed some common flow patterns, but the material flow was also found to be not symmetric to the weld centerline. While a high amount of tracer material was moved to the back of its original position, only a small part was moved to the front. Furthermore, a well defined interface was encountered between advancing and retreating side. A downward movement occurred at the advancing side around the pin diameter, while the material at the retreating side was rather moved to the top. The authors thus suspected, that the actual stirring only occurred in the area below the tool shoulder, where the material is directly influenced by the rotation.

In another investigation Guerra et al. [GSM⁺02] used a thin copper foil, which was placed along the faying surface of the weld, and at the end of the process the pin was stopped manually to achieve the pin to be frozen within the workpiece. Metallographic examinations were carried out as shown in the cross-section in figure 2.18a. The sections were etched with Keller's reagent for 60 s to visualize the dark features. The dark areas consist of fine grains and thus were subject to high deformation degrees. In the cross-section in figure 2.18b it can be seen, that these areas are much more pronounced on the advancing side. On the retreating side grey areas (figure 2.18a, (C)) can be encountered, which are twice as thick as on the retreating side. Guerra et al. [GSM⁺02] describe them as the "transition zone" where the material rotates with a decreased velocity. As also shown in figure 2.18b, copper particles torn from the foil only appeared in the darker areas/ rotational zones.

Guerra et al. [GSM⁺02] determined two basic processes for the material flow:

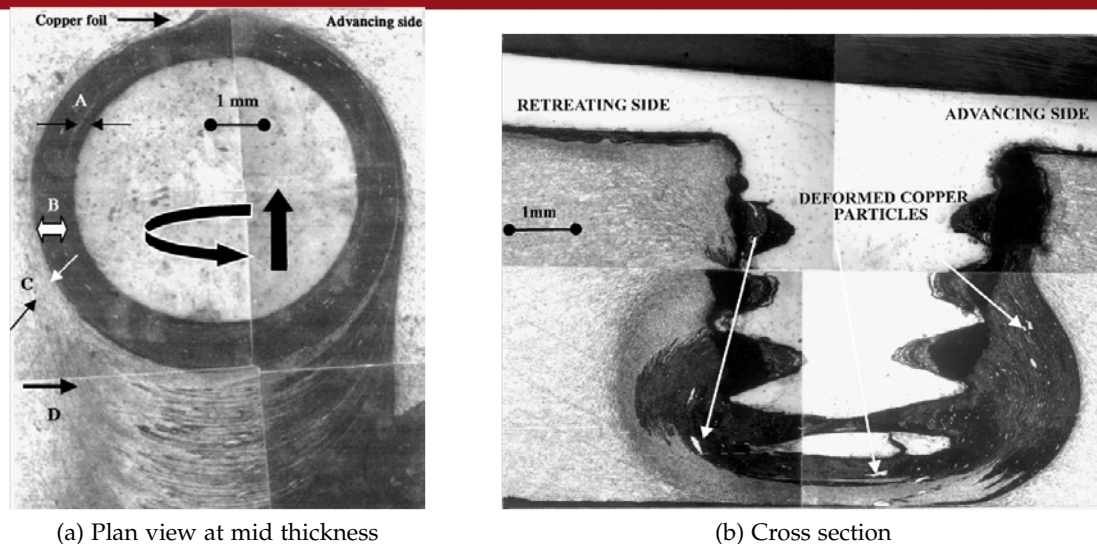


Figure 2.18: Plan view and cross-section of a "frozen nib" [GSM⁺02]

- The material on the advancing side of the pin is moved into an area, that rotates and advances with the pin and is then sloughed off behind the pin "in arc-shaped features". Thus high deformations and shear stresses are applied on the material, leading to high hardness values (95HV) in the area.
- The material on the retreating side however is extruded around the pin, but does not rotate around it, therefore showing much lower hardness values (35HV).

Furthermore he described the upper third of the weld to be mainly influenced by the shoulder movement while large vortex movement is caused by the threads in the rotational zone.

2.1.5.3 Simulation

Several simulations were carried out to predict temperature distribution, strain rates, material flow and forces during FSW/FSP. Li et al. [LMH10] used an advanced Finite Element (FE) model to describe the complex interaction of plastic deformation, flow transportation, mechanical stirring, heat generation etc. The material movement was visualized by defining tracer particles at different locations (See Li et al. [LMH10]). A single plate was used for simulation to provide a continuum model. The tracer particles were placed in lines along the weld.

From figure 2.19 it can be seen, that the particles, which came in direct contact with the tool pin, experienced a much higher displacement in a short time than the particles aligned on the retreating side. Some particles in the contact area of the retreating side did not rotate with the shoulder and remained there. Furthermore, an arc-shaped strip was formed behind the tool as seen in prior investigations. In general, the shoulder movement dominated the material flow in this investigation as the tracer particles were placed near the surface.

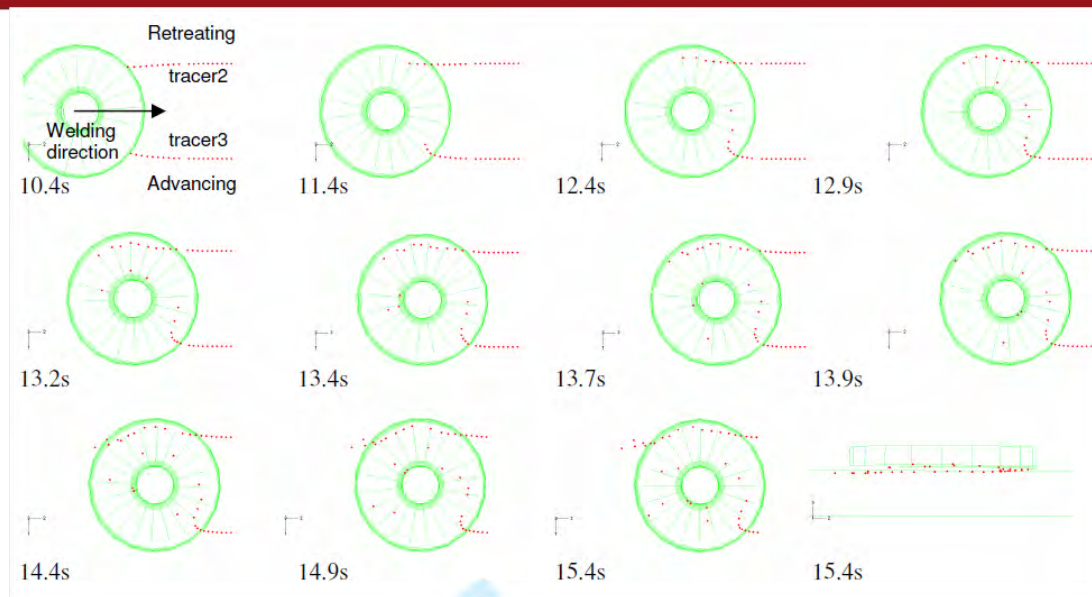


Figure 2.19: Positions of the tracer particles at different time points [LMH10]

Investigations of Zhang [ZZ08] also showed, that the material flow near the top surface is significantly influenced by the shoulder rotation and that the material on the retreating side does not rotate around the tool. He also described the distance between the arc-shaped rings behind the tool to be equal to the transversal movement of the tool after one rotation.

Tutunchilar et al. [THG⁺12] developed a 3D Lagrangian incremental finite element method (FEM) simulation and obtained three-dimensional results of the material flow patterns in cast Al-Si alloy by using the software DEFORM-3D for point tracking during deformation. Like applied in prior investigations he used a tool with a threadless pin. To visualize the material flow, a groove with a depth of 3 mm and a width of 1 mm, respectively, was cut into an actual workpiece and filled with graphite powder. The tool with a shoulder and pin diameter of 18 mm and 6 mm, respectively, was used for FSP. The probes were examined via metallography and the results "compared with those acquired via experiment in order to validate the accuracy of the developed simulation" [THG⁺12].

In the simulation, the tracking points were placed into different depths of workpiece as shown in figure 2.20. The simulation was then carried out comparing the track of the points placed at the center line, advancing side and retreating side. Figure 2.21 shows the flow patterns of the points at the center line of the weld. Due to the influence of the shoulder rotation, the points closer to the surface are subjected to a high displacement and stretched towards the advancing side. The points near the bottom only show a semicircular movement from the retreating towards the advancing side, but never revolve around the tool (See Tutunchilar et al.[THG⁺12]).

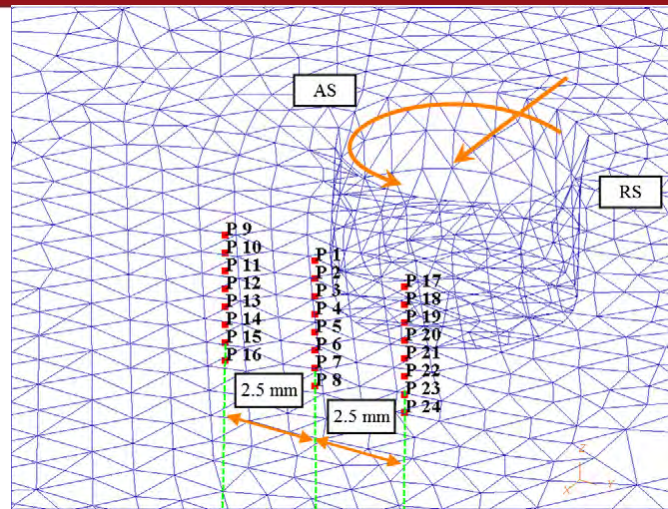


Figure 2.20: Initial positions of points, that have been selected for material flow in the stir zone [THG⁺12]

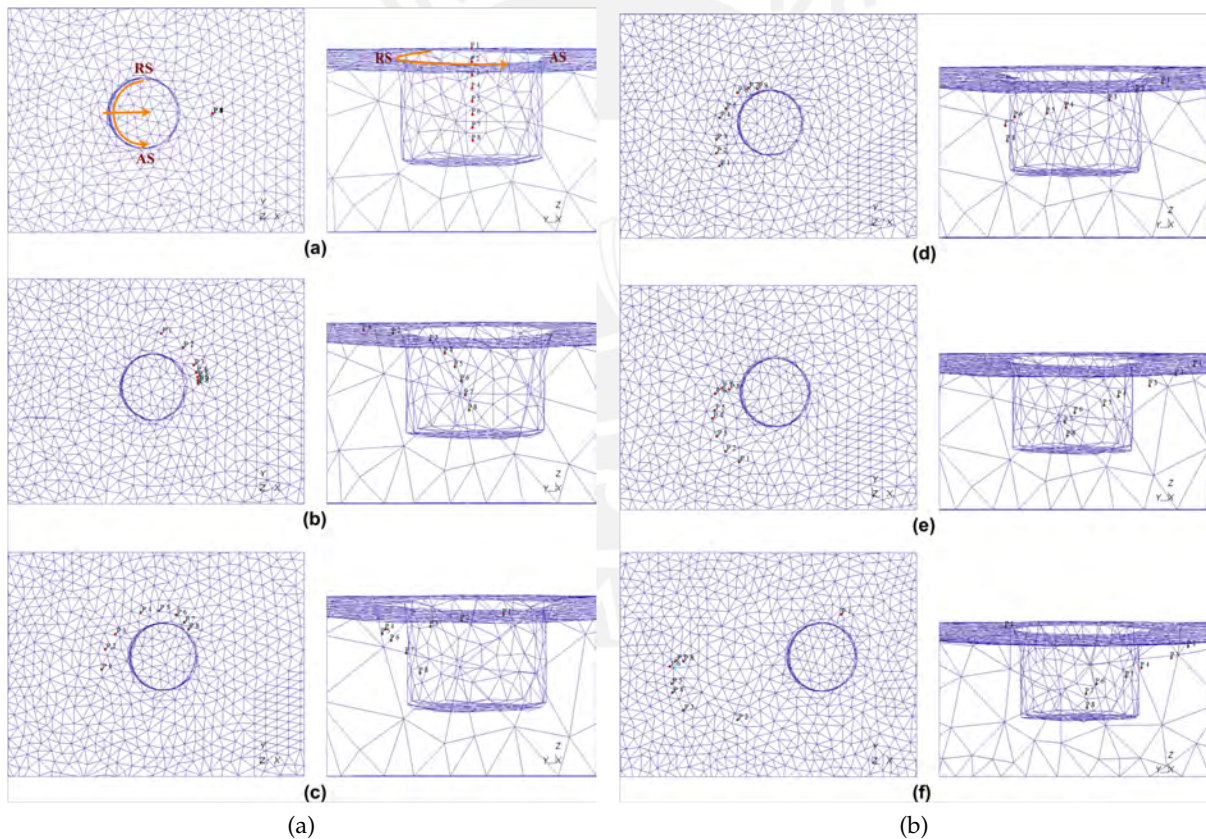


Figure 2.21: Flow patterns of points at the center line [THG⁺12]

The simulation also revealed, that the velocity of the point movement decreases, the closer the points were placed to the bottom, which is caused by the frictional shear force induced by the tool shoulder. Moreover the velocity at the retreating side is slightly higher than on

the advancing side, which is due to the superposition of rotational and transversal movement. Another phenomenon is, that points near the tool shoulder on both retreating and advancing side and as well at the center line are moved to the advancing side as a final position. Thus the widely reported agglomeration of embedded powder or tracer particles near the surface at the advancing side can be explained. Tutunchilar et al. [THG⁺12] propose, that shifting the tool towards the retreating side could lead to a better distribution of particles in composites.

2.1.5.4 Influence of the tool geometry

Investigations of Zhao et al. [ZLQW06] on the influence of the tool profile on the material flow were carried out by using marker insert technique (MIT). Therefore the marker material was filled into inserts, which had been placed on both retreating and advancing side at three different heights. 3D-Plots of the material flow were then obtained by milling off successive slices from the top to the bottom of the weld and combining the data of the metallographic images.

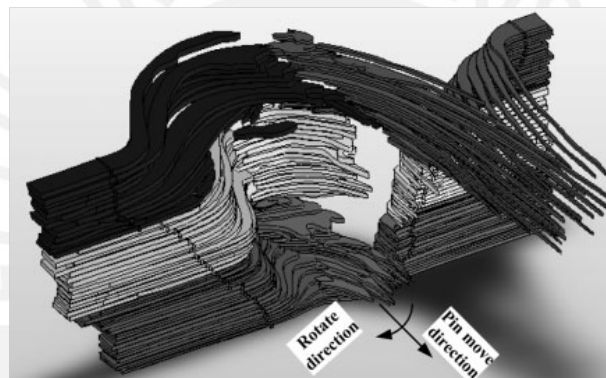


Figure 2.22: 3D plot of markers flow [ZLQW06]

As seen in other investigations, common flow patterns and differences of the flow at advancing and retreating side were encountered as shown in figure 2.22. It shows for example, that only on the advancing side, material was moved forward compared to its original position and that the shoulder movement causes an increased material flow at the top of the weld, as mentioned by other authors. To investigate the influence of the tool geometry, the 3D plots of three different tool geometries were created. Therefore a cylindrical, a taper and a threaded, taper pin were used for FSW and the results were compared as shown in figure 2.23 and figure 2.24. Furthermore the cross sections were compared as shown in figure 2.25.

While the plots of figure 2.23 show similar, common flow patterns, the main differences between the tools can be encountered in the vertical flow. Only when using the threaded, taper pin, a significant vertical material flow was obtained. As shown in figure 2.24 the material was pushed downwards on the advancing and lifted on the retreating side. Figure 2.25 shows hole defects on the lower part of the advancing side when using column and taper pins, while welds with the threaded pin did not show these effects. Zhao et al. [ZLQW06] identified insufficient

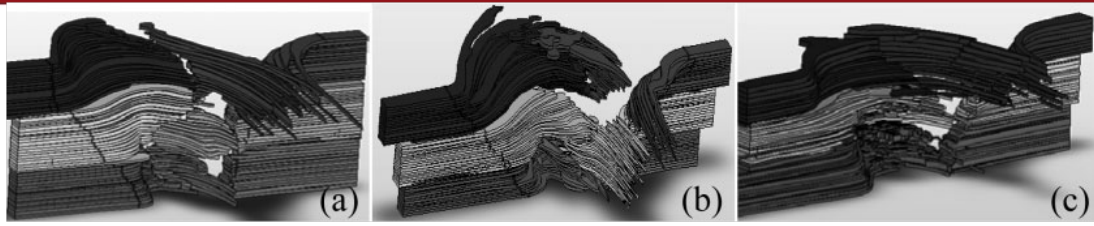


Figure 2.23: 3D plot of markers flow welded by: (a) column, (b) taper and (c) threaded, taper pin [ZLQW06]



Figure 2.24: Vertical mixing in weld using: (a) column, (b) taper and (c) threaded, taper pin [ZLQW06]

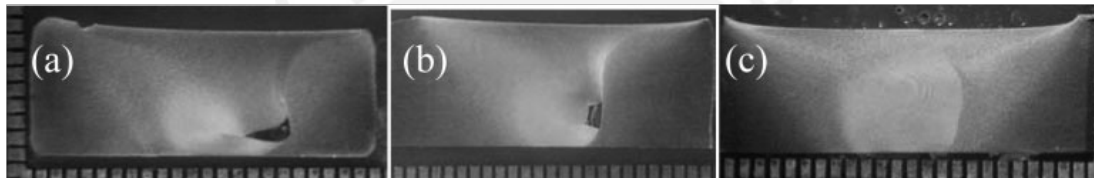


Figure 2.25: Cross-section views of FSW zone: (a) column, (b) taper and (c) threaded, taper pin [ZLQW06]

material flow as a cause for the defect formation. As shown in figure 2.26 the flow pattern of column and taper pin is prone to void formation as a point of minimal transport against the welding direction occurs in the middle of the weld, while it can be encountered on the bottom, when the threaded pin is used.

Kumar and Kailas [KK08] examined the influence of the tool by linearly increasing the interference between tool and workpiece. Therefore the backing plate in their experimental setup showed a small inclination towards the welding direction. Thus the contact surface between tool and material gradually increased during the transversal motion of the tool. As shown in figure 2.27, the increase of the interference caused a decrease of the defect size and occurrence in the weld. At the same time the weld was found to be asymmetric, when a certain axial load was exceeded. Kumar and Kailas [KK08] described this phenomenon to be caused by the increased influence of the tool shoulder, moving material away from the retreating side to the weld nugget area. In general they divide the material flow during FSW into two processes:

- *Shoulder driven material flow*: The material moves from the retreating to the advancing side and forges against or bonds with the colder base material. The authors describe this flow as "the effectiveness of the shoulder to keep the material in the weld cavity" [KK08],

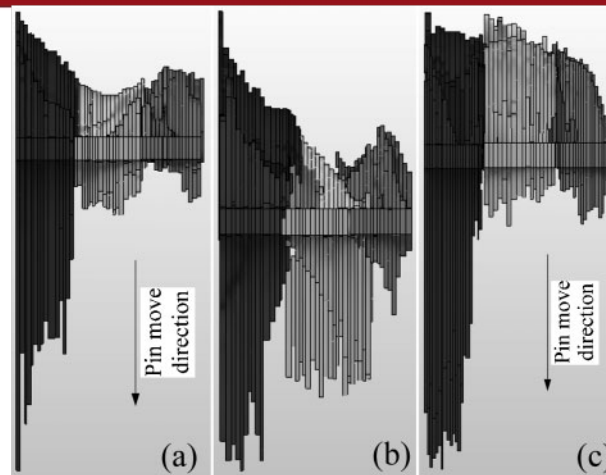


Figure 2.26: Right hand plot of markers flow welded by: (a) column, (b) taper and (c) threaded, taper pin [ZLQW06]

- *Pin driven material flow*: The material flows and forms layers around the pin and a cavity is created during plunging. The boundaries are eliminated, when the two material flows interact. The pin driven flow is described as "the effectiveness of the pin to constrain the transferred material in the weld cavity" [KK08].

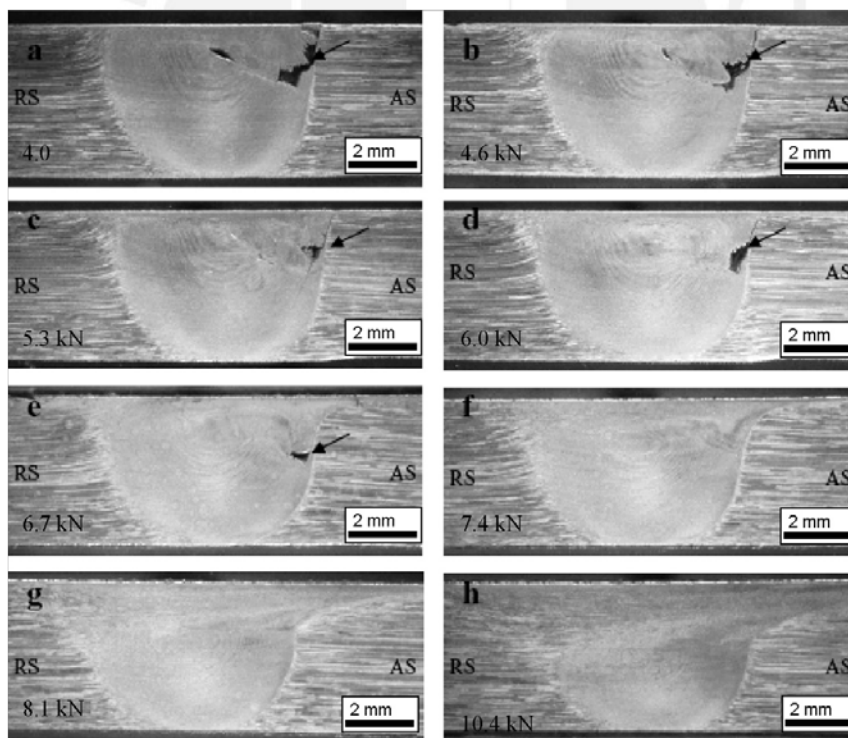


Figure 2.27: "Evolution of a defect-free weld as a function of the shoulder interaction with the base material" [KK08]

Hirasawa et al. [HBO⁺10] compared different tool geometries for friction stir spot welding using the particle method approach. Thus, the material flow patterns for using a tapered pin, inverse tapered pin, triangular pin, convex shoulder, and concave shoulder were modeled. When the triangular pin was used, an enhanced material flow was encountered. Figure 2.28 shows, that during the rotation of the pin, the direction of the material flow constantly alternates, thus providing an increased mixing effect.

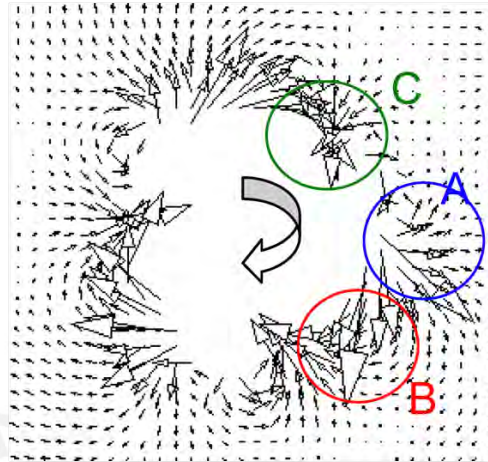


Figure 2.28: Plan view on the material flow pattern using a triangular pin [HBO⁺10]

Investigations of Elangovan et al. [EBV08] were carried out to obtain the influence of the tool profile and axial force on the resulting FSP zone. "Five different tool pin profiles (straight cylindrical, tapered cylindrical, threaded cylindrical, triangular and square)" [EBV08] were used to produce joints at different axial force levels and the results were compared by tensile testing and metallographic examination. All joints fabricated by threaded cylindrical, triangular and square pins were found to be defect free at any axial force while straight and taper cylindrical pins produced defects at low axial force. Figure 2.29 shows the macrostructure of the joints produced by the square pin. Tests on the mechanical properties of the different joints revealed, that using a square pin profiled tool leads to superior tensile properties, increased microhardness and uniform, very fine grained microstructure. The authors concluded that the flat faces of "triangular and square pin profiles produce a pulsating stirring action in the flowing material" [EBV08], which does not occur when using tools with cylindrical or taper pin profiles.

Nearly the same experimental procedure was used in another investigation by Elangovan and Balasubramanian [EB08], but instead of the axial force, the joints were produced using different shoulder diameters. Again, the square probe showed superior tensile properties, as the "higher number of pulsating action experienced in the stir zone" [EB08] leads to finer microstructure. Hence higher yield strengths could be obtained.




Axial Force (kN)	Macrostructure		Size of FSP zone (mm)		Shape of FSP zone	Name of the defect and location	Quality of weld metal consolidation	Probable reason
	RS	AS	W	H				
6			11.3	5.7	Inverted Trapezoidal	No defect	Good	Sufficient flow of the metal by pulsing action of the pin profile
			6.7					
			4.1					
7			12.1	5.6	-do-	-do-	-do-	Eccentricity of the pin profile causes dynamic orbit with associated pulsating action resulted in good weld.
			6.7					
			4.6					
8			11.8	5.9	Inverted Trapezoidal with shear lips	-do-	-do-	Excess heat input due to additional axial force reduces thickness of the plate in the weld zone
			7.1					
			5.3					

Figure 2.29: "Macrostructure of the joints fabricated by square pin profiled tool" [EBV08]

2.1.6 Defect characterization

There are several defects, that can be encountered, when friction stir welds are produced under suboptimal conditions. According to Arbegast [Arb03], FSW defects are related to processing temperatures, metal flow patterns and joint geometry. They can be classified as shown in figure 2.30. A few selected defects are defined below.

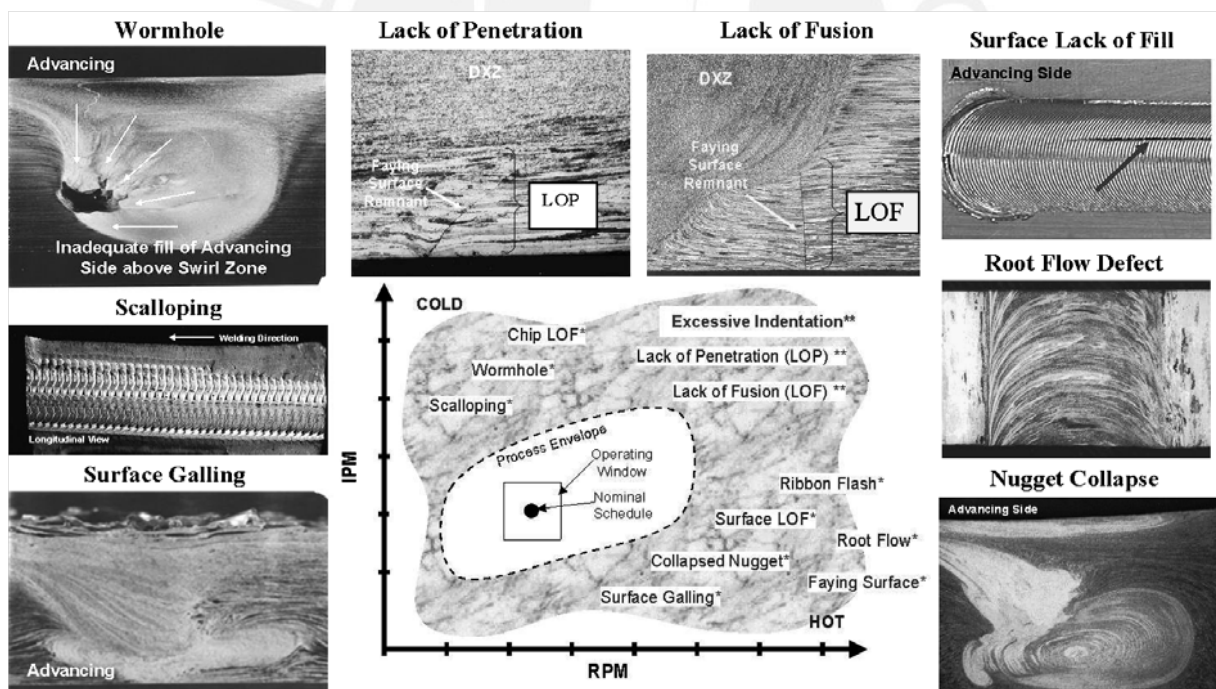


Figure 2.30: Characteristic defect types in friction stir welds [Arb08]

- *Wormhole Defects:* tunnels formed on the advancing side, which form due to insufficient material flow. This can be caused by high travel speed at relatively low rotational speed, thus leading to a cold weld.

- *Ribbon Flash*: "Excessive expulsion of material on the top surface leaving a corrugated or ribbonlike effect along the retreating side" [Arb03]. It occurs, when the weld gets excessively hot due to high forge loads, high plunging depths or different thicknesses of retreating and advancing side.
- *Surface Lack Of Fill*: "A continuous or intermittent top surface void on the advancing side" [Arb03] occurs because of insufficient flow arm formation, forge pressure or plunging depth.
- *Surface Gallling*: This "galling and tearing of the metal on the top surface of the weld beneath the pin tool" [Arb03] is also due to a too hot weld, which causes metal to be sticking to the pin.

Another typical feature is the formation of so called "onion rings" in the weld nugget. They are formed because the pin-driven material carries layers of plasticized material and when it interacts with the shoulder-driven material the layers are joined and deposited in the weld. Due to a different degree of deformation they show different etching behaviour and can thus be distinguished (See Kumar and Kailas [KK08]).

2.2 Carbon Nanotubes

Carbon nanotubes (CNTs) were discovered by Sumio Iijima in 1991 and have been subject to several investigations since then. The reason for this is their wide range of outstanding properties, such as high specific tensile strength, stiffness and Young's modulus, good wear resistance and damping properties but also their incredible electrical and thermal properties show potential for various applications. They are usually produced by carbon-arc discharge, laser ablation of carbon or chemical vapor deposition.

2.2.1 Structure and properties

There are two main types of CNTs: single-walled carbon nanotubes (SWCNTs), which consist of a "single graphite sheet seamlessly wrapped into a cylindrical tube" (See figure 2.31 (A-D)), and multi-walled carbon nanotubes (MWCNTs), that "comprise an array of such nanotubes that are concentrically nested like rings of a tree trunk" [BZH02]. The diameter can range from 0.4 nm to 3 nm for SWCNTs and from 1.4 nm to 100 nm and more for MWCNTs.

Depending on the direction of the sheet wrapping, SWCNTs are either metallic or semiconducting. Due to the weak coupling of the sheets in MWCNTs, their electrical properties are similar to those of SWCNTs. The one-dimensional structure of the CNTs allows them to carry high currents up to $4 \cdot 10^9$ A/cm² over long distances, practically without heating. Thermal conductivity also reaches exceptional values. 3000 W/(m K) to 6000 W/(m K) have been measured on

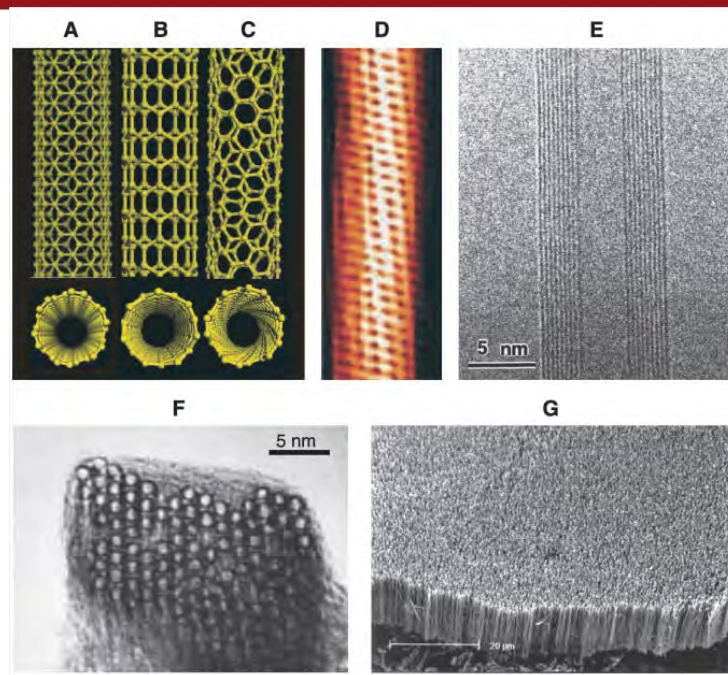


Figure 2.31: Schematic illustrations of different SWCNT structures (A-C), Tunneling electron microscope image (D), TEM and SEM images of MWCNTs (E-G) [BZH02]

single CNTs, thus exceeding the values of natural diamond and the basal plane of graphite (See Baughman et al. [BZH02]). At the same time, they show a very low coefficient of thermal expansion ($CTE \approx 0$), which makes them very suitable for thermal management applications. Furthermore, their mechanical properties even exceed those of carbon fibers. Stiffness values up to 1000 GPa and strength in the range of 100 GPa combined with an extremely low density make them the strongest fibers known to mankind (See Bakshi et al. [BLA10]).

2.2.2 Application in Metal Matrix Composites

In the last years, many investigations were carried out on reinforcing various materials like plastics, ceramics and metals with CNTs in order to enhance mechanical, thermal or electrical properties. For metal matrix composites (MMCs) the most investigations focus on the enhancement of mechanical properties like wear, strength and so on, but the influence of CNTs on electrical, vibrational and thermal properties has also become a point of interest.

Figure 2.32 shows different processes, which are applied to fabricate CNT-reinforced MMCs. At the moment, powder metallurgy is the most popular fabrication method, followed by electrochemical deposition for applying thin coatings of CNT composites on metal or applying metal on CNTs. A homogeneous distribution of the CNTs in the matrix still represents the biggest challenge as CNTs show a natural tendency for agglomeration. Furthermore, high

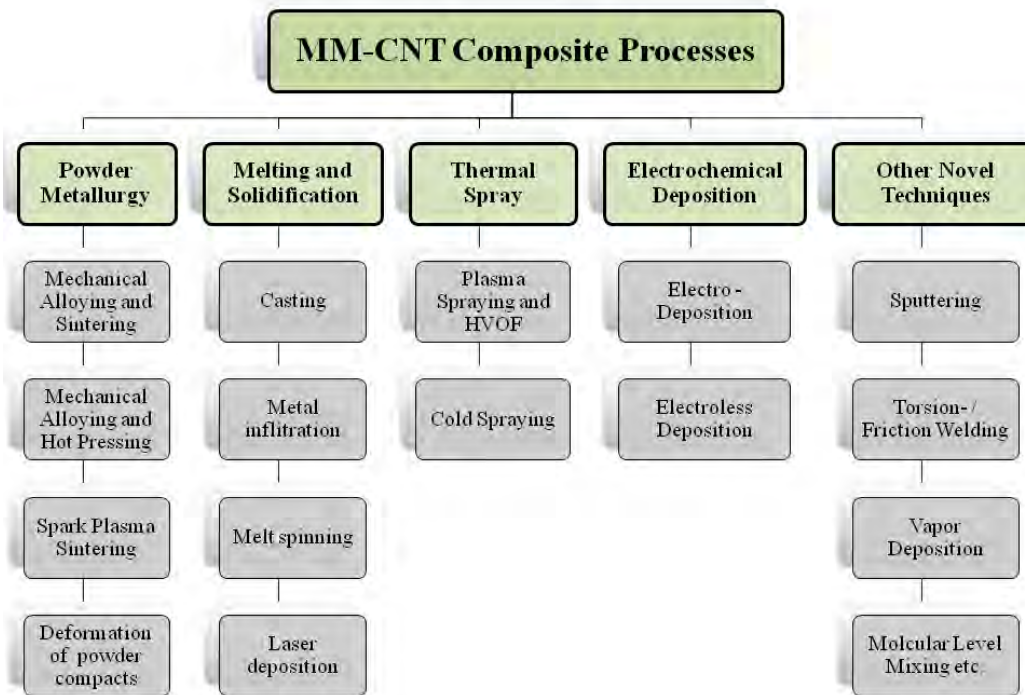


Figure 2.32: List of different processing routes for Metal Matrix-CNT composites (See Baughman et al. [BZH02])

temperatures during sintering or high deformation rates during ball milling can damage the tubular structure of the nanotubes and has to be considered as well.

When using powder metallurgy for composite fabrication, the CNTs have to be mixed with metal powder first before the process of compaction and sintering or hot pressing follows. As a good dispersion of the CNTs should be obtained, the compacts are often subjected to post-process deformation like rolling, extrusion or similar processes. Electrochemical deposition however is only used for thin coating of 20 μm to 180 μm and mainly applied for Ni or Cu based composites. Other processes also show promising results and are constantly developing.

CNTs show higher strength and stiffness than metals, which is why they are incorporated into the metal matrix. To understand the strengthening mechanisms, the shear lag model, which is also used with conventional fibers, is applied to evaluate the properties of the composite. Therefore, the interface between CNT and base metal plays an important role, as it is responsible for stress transfer (See Baughman et al. [BZH02]). But the uniform dispersion is even more important and also difficult to achieve, as CNTs form clusters due to van der Waals forces and their high surface area. This clustering leads to the concentration of reinforcement at certain points and can worsen mechanical properties. Thus, avoiding this effect is a main point of research. Ball milling was found to be effective, but also spray drying or even a CVD method to grow CNTs on Al powder obtained good dispersions.

Another application for CNTs in MMCs is to improve electrical and thermal properties. As mentioned in section 2.2.1, they reach exceptional values in this field. Investigations have been carried out on reinforcing Cu and Ag with CNTs but no decrease in electrical resistivity could be encountered. This was attributed to clustering and strain effects in the metal matrix, which both hinders the electron transfer through the composite (See Baughman et al. [BZH02]). However regarding the CTE, Tang et al. [TCZC04] for example obtained a decrease of up to 65% by fabricating SWCNT/Nano-Al-composites with powder metallurgy using a volume fraction of 15 vol.%. Other investigations were carried out in order to increase the thermal conductivity, but only a few succeeded as an increase in CNT volume fraction also leads to more pores, thus again depending strongly on the dispersion of the CNTs in the matrix and their bonding among each other.

Chu et al. [CGJ⁺10] produced MWCNT/Cu-composites by a novel mixing procedure called particle compositing process, where "the powder mixture is subjected to the high inter-particle collision in a high-speed air flow", followed by spark plasma sintering. In spite of the fact, that the thermal conductivity of the CNTs is about ten times higher than that of Cu, the thermal conductivity of the composite was always found to be below that of the pure Cu sample. The authors considered this result to be caused by the interfacial resistance between the CNTs and the Cu matrix, which impedes the heat flow, as well as remaining porosity. Furthermore they assumed, that the CNTs rearrange during grain growth towards the boundaries and accumulate as the volume of grain boundaries decreases during sintering as shown in figure 2.33. Hence, the thermal conductivity decreased, even if the CNTs were uniformly dispersed in the powder.

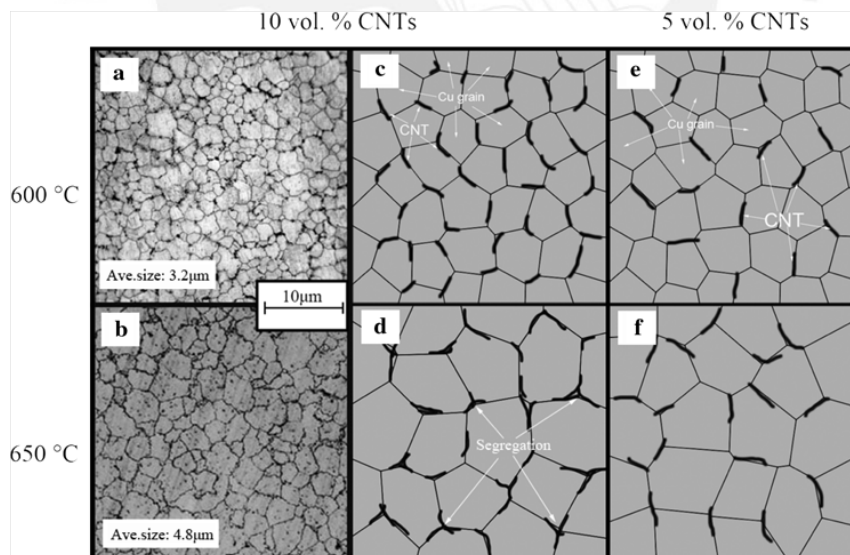


Figure 2.33: "Distribution of CNTs at the Cu grain boundaries at different sintering temperatures and CNT contents" [CGJ⁺10]

2.3 Synthesis of CNT-Aluminum composites by FSP

In order to decrease processing steps and time as well as to provide a wider range of possible applications for CNT-aluminum alloy (Al) composites, Johannes et al. [JYS⁺06] investigated the survivability of SWCNTs during FSP. Therefore holes were drilled at different locations along the processing direction and filled with SWCNT powder. Then, the process was performed with 400 rpm and 25.4 mm/min. The samples were tensile tested to obtain a fracture surface for SEM examination. As shown in figure 2.34, the CNTs survived the high temperatures and strain rates during FSP except minor local damages, but problems with clumping and bundles occurred.

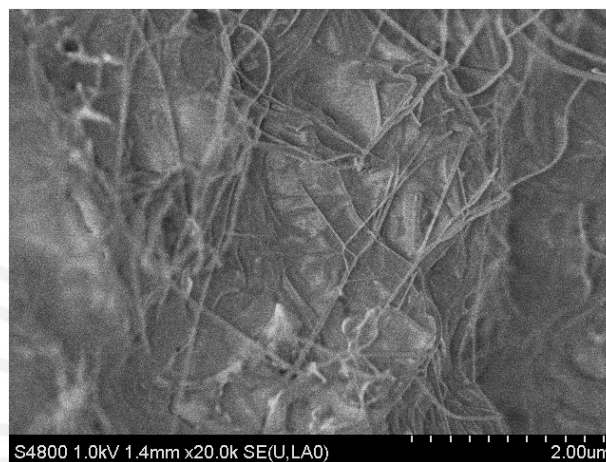


Figure 2.34: SEM images of CNTs incorporated into the Al matrix by FSP [JYS⁺06]

Lim et al. [LSG08] filled the powder into a shallow groove and covered the Al plate with a top sheet to keep the CNTs within the groove during FSP. A cylindrical pin with an M4 thread was used to simplify flow analysis and the tool was rotated counterclockwise to obtain a downward flow of the material. Furthermore the shoulder plunging depth was varied. As shown in figure 2.35, the best distribution was achieved with a high shoulder penetration but even then lamella and fissure formation was encountered. As revealed by SEM examination, the fissures contained large amounts of entangled CNTs, which were not embedded into the matrix. Microhardness measurements also confirmed, that the CNTs were not dispersed uniformly.

In order to fabricate an Al based MMC with increased thermal conductivity, Luick [Lui09] filled an Al tube with CNT powder. The tube was sandwich pressed between to Al plates and then subject to three pass FSP. After that the samples were cold rolled, which led to severe cracking in the samples. Hence no increase in thermal conductivity could be obtained.

As prior investigations suggested, that a homogeneous distribution of CNTs may not be achieved in just one FSP pass, Izadi and Gerlich [IG12] used multipass FSP for the composite fabrication. They also filled a groove with powder, but sealed the surface with a pinless tool before FSP was performed. Three passes were then performed, using different tools and parameters. Thus

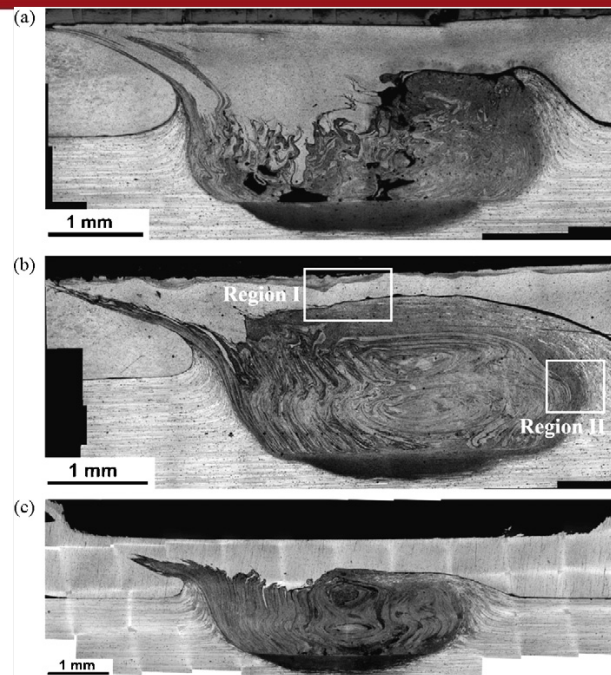


Figure 2.35: "Optical micrographs of friction stir processed regions processed with (a) 1500rpm and 0.03mm of shoulder penetration, (b) 1500rpm and 0.24mm of shoulder penetration and (c) 2500rpm and 0.24mm of shoulder penetration" [LSG08]

a uniform particle and microhardness distribution with high peaks in hardness was obtained as shown in figure 2.36, with no evidence of lamella, flow arm or onion ring formation. Like reported in other investigations, TEM analysis revealed micron grain sizes of $1\ \mu\text{m}$ to $2\ \mu\text{m}$ after 2 passes and less than half as big after 3 passes. This is considered to be caused by CNTs pinning to the grain boundaries and thus retarding grain growth. In figure 2.37 it can be seen, that a lot of CNTs were found to be damaged after two passes and some already had transformed to circular carbon structures. After three passes the structure mainly consisted of polyaromatic carbon structures, which form when the outer walls transform into graphitic shells and "curl up into spheroidal structures in order to eliminate dangling bonds" [IG12].

Liu et al. [LXWM12] combined powder metallurgy and FSP to obtain singly dispersed CNTs in the Al matrix. Therefore, the CNTs were mixed with an Al alloy powder, ball milled for 8 hours, hot pressed to billets and then hot forged into disc plates before one or four pass FSP was carried out. Optical microscopy showed layer formation of particle-rich and particle-poor zones in the nugget after one pass, which are considered to form, when the material is "extruded downward along the pin wall" and the pin continues its transversal movement. After four passes no clusters or layers were encountered and the CNTs were found to be dispersed along the grain boundaries, but they had also been damaged and shortened up to 400 nm. The formation of very fine grain due to the pinning of the CNTs to the grain boundaries was observed as well and an increase in yield strength was obtained.

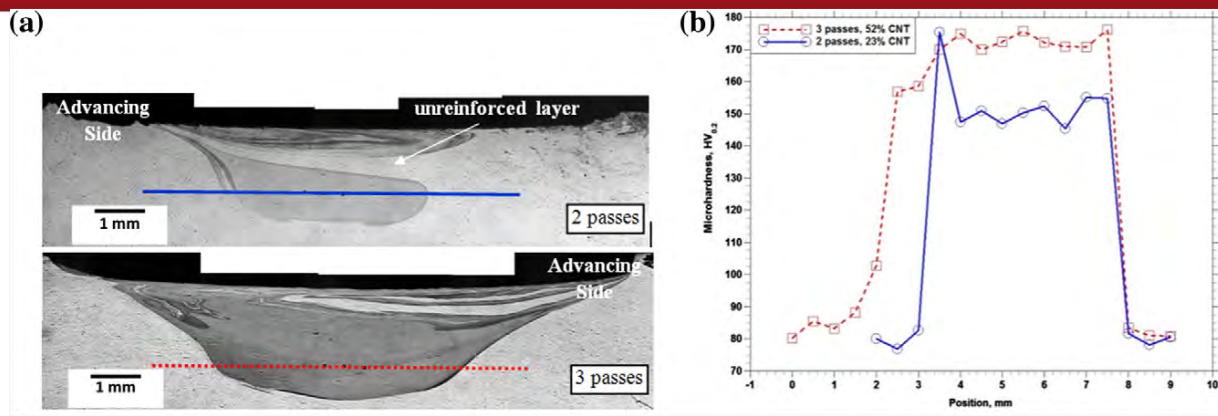


Figure 2.36: (a) Cross section of FSP zone using two and three passes and (b) corresponding microhardness profiles [IG12]

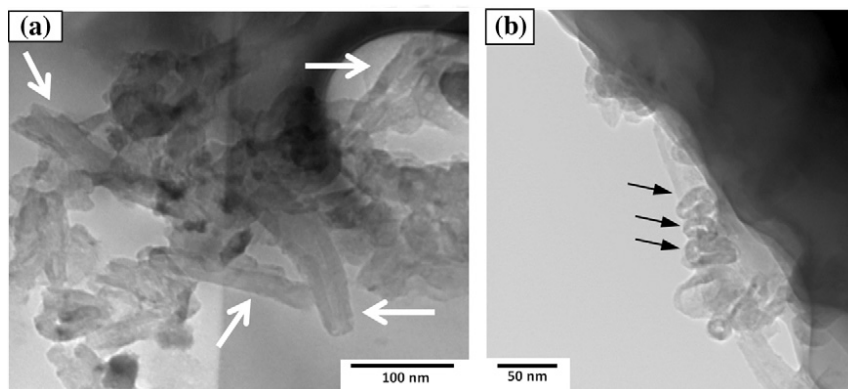


Figure 2.37: TEM micrographs of the composite showing (a) extensive damage of the CNTs after two passes and (b) formation of circular carbon structures [IG12]

In another investigation by Liu et al. [LKL⁺12], holes with different depths were drilled into an Al plate along the processing direction to obtain different volume fractions. The FSP was carried out using five passes. A uniform distribution could be achieved with layers only to be formed in the thermo-mechanically affected zone (TMAZ). Furthermore TEM analysis showed a good interfacial bonding and wetting between MWCNTs and matrix, but breakage and damage also occurred (no information about the amount). The maximum tensile strength of the composite was found to be two times higher than that of the Al matrix.

Table 2.1 gives a summary of the investigations carried out on CNT-Aluminum alloy composites by FSP, also showing used tool profiles and processing parameters. Comparing them, it is obvious, that with one pass, it is difficult to achieve a uniform distribution but after more than two passes, the tubular structure of the CNTs is damaged or even destroyed. On the other side it can be noticed, that only conventional tool profiles were used for the experiments, in spite of the fact, that investigations on the influence of the tool profile propose other geometries like square profiles for an increased mixing effect as described in section 2.1.5.4.

Table 2.1: Summary of investigations on CNT-Al composites by FSP

Investigation	Tool profile	Welding parameters	Experimental setup	Results
[JYS ⁺ 06]	n/a	400rpm, 25.4 mm/min	hole drilled into a Al plate and processed	CNTs survived the process, little damage occurred
[LSG08]	cylindrical, threaded pin, Ø4 mm	1500-2500rpm, 150 mm/min, 0.03-0.24mm plunge	channels filled and covered by a top sheet before FSP	good distribution with high plunge, fissure and lamella formation
[Lui09]	tapered spiral	1400rpm, 150 mm/min	sandwiching of a powder filled tube, FSP, cold and hot rolling	severe cracking in the samples due to rolling process
[IG12]	cylindrical, threaded, Ø4 mm	(454, 1130)rpm, 30 mm/min	MWCNT filled and sealed groove was processed in three passes	some CNTs damaged after two passes, almost all after three
[LXWM12]	concave shoulder, threaded cylindrical pin, Ø6 mm	1200rpm, 100 mm/min	CNTs mixed with Al powder, ball milled for 8 hours, hot pressed and hot forged before one or four pass FSP	CNT damage and shortening, fine grain formation, no layers after four pass
[LKL ⁺ 12]	cylindrical, Ø12 mm	950rpm, 30 mm/min	drilled holes of different depths, five passes	good interfacial bonding but also CNT damage and breakage, increased tensile strength

3 Objective

Due to their outstanding properties, the incorporation of CNTs into MMCs offers opportunities for several applications, like enhancement in mechanical, thermal or electrical properties of the composite. The key for the success of these applications is the uniform distribution of the CNTs within the metal matrix. Investigations using several techniques like sintering, electrochemical processes and so on have shown progress in this field, but it still remains a mayor challenge.

Friction stir processing has recently been applied to disperse CNTs into bulk aluminum alloy plates. A homogeneous dispersion was obtained after multipass FSP but this technique leads to damage within the tubular structure of the CNTs, as their survivability during the severe deformation and high temperatures is limited to a low number of passes.

Several investigations on the material flow during FSW/FSP have shown, that welding parameters and especially the tool geometry play a critical role for the resultant formation of the joint. For example, it is reported, that a threaded tool pin provides vertical mixing while a pin profile with flat faces like a triangular pin generally leads to an increased mixing effect. This is because flat faces act like paddles and produce a constant alternation of the material flow direction, which also shows potential for dispersing particles in MMCs. In spite of this fact, most investigations on particle reinforced MMCs by FSP are carried out with conventional FSW tools. Usually, cylindrical or taper pins with threads are used, though the two processes may require different material flow behaviours.

Therefore the objective of this thesis is to compare different tool profiles under different processing parameters to obtain a uniform distribution of CNTs within the aluminum matrix with a minimum number of process steps. Tools with a cylindrical, triangular, square and nearly cross-shaped pin profile will be used, all of them with an M4 thread incorporated. Thus the share of turbulent flow and pulsating action within the material flow shall be increased and finally lead to a better dispersion of the particles in one pass. Shallow grooves of $1\text{ mm} \times 1\text{ mm}$ will be filled with Ethanol wetted MWCNT powder, sealed with a pinless FSW tool to avoid the powder being pushed out during processing and then be subjected to one pass FSP. The results will be compared by carrying out metallography and microhardness measurements for cross and longitudinal sections, SEM analysis of the fracture surfaces and electrical resistance measurements along the joint.

4 Experimental Procedure

4.1 Base materials

To fabricate the CNT-Al composites, Al 5086 plates with a thickness of 12 mm were used as matrix material. Table 4.1 shows the chemical composition of this alloy. Channels with cross section of 1 mm \times 1 mm and a length of 110 mm were cut into the surface of the plates using a blade saw. Figure 4.1 shows a cross section of the base material. The little, black spots are iron-rich phase precipitations.

Table 4.1: Chemical composition of Al 5086 according to DIN EN 573-3

	Si	Fe	Cu	Mn	Mg	Cr	Zn	Ti
%	0.4	0.5	0.1	0.2 to 0.7	3.5 to 4.5	0.05 to 0.25	0.25	0.15

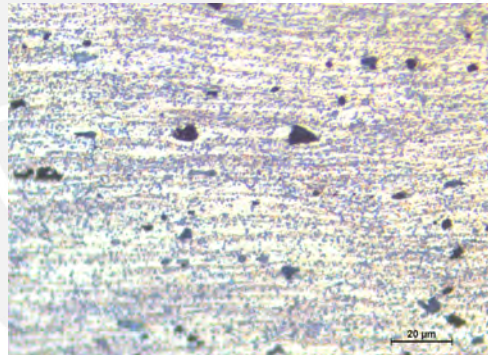


Figure 4.1: Cross section of the base material

CVD produced multiwalled CNTs (MWCNTs), purchased from Sigma Aldrich (Product No. 659258), with diameter ranging from 110 nm to 170 nm and length ranging from 5 μ m to 9 μ m were used for the experiments. Figure 4.2 shows the CNTs in their as-received condition, as an agglomerated powder and entangled to each other.

4.2 Sample preparation

The CNT powder was put onto the plate, wetted with a small amount of ethanol to facilitate the filling of the channels and then pressed into the channels manually, using a thin metal sheet.

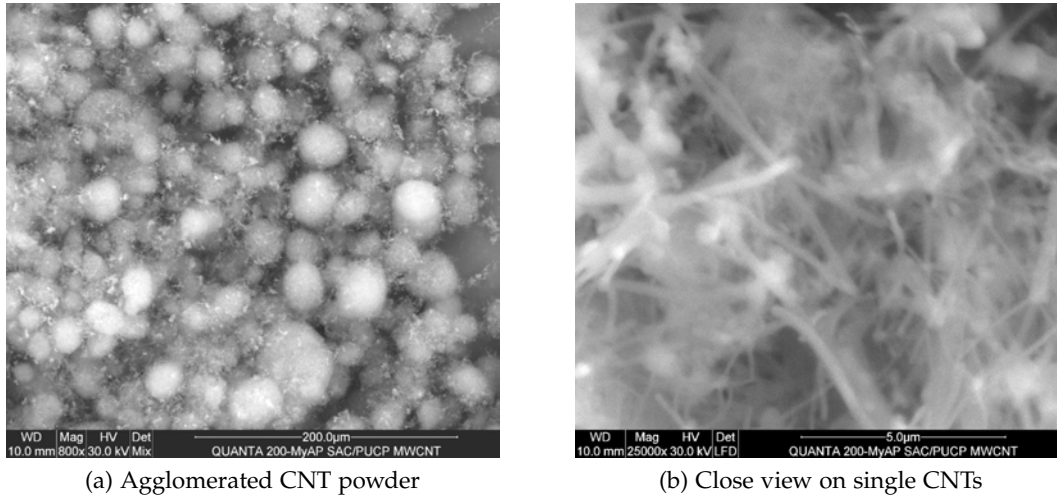


Figure 4.2: MWCNTs in as-received condition

Figure 4.3 shows an example of the filled channels. The wetting and pressing was done to prevent the powder from being blown out during the process due to its low density and also to provide a high volume fraction within the processed area.

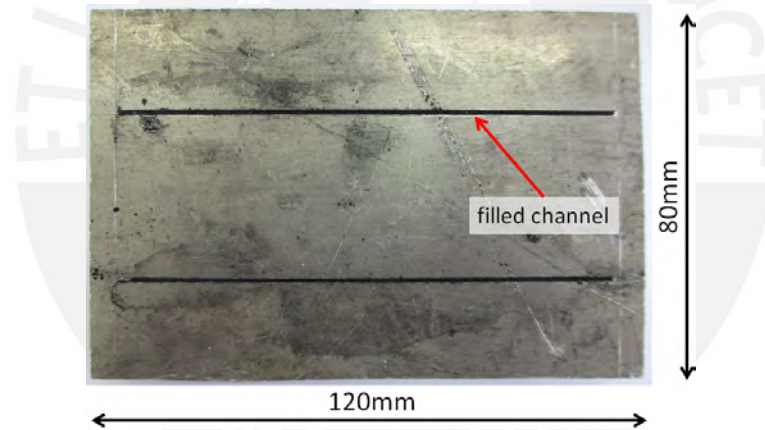


Figure 4.3: Channels filled with ethanol wetted CNT powder

Four tools with different pin geometries were fabricated to compare their performance regarding the CNT distribution. The tools were fabricated of BOHLER K340 ISODUR tool steel and subjected to a heat treatment to increase their hardness to approximately 55 HRC. Therefore they were preheated at 500 °C for 20 min, heated at 1050 °C for 45 min, quenched in oil and subjected to posterior annealing at 500 °C for 80 min and 60 min. The tool profiles are illustrated in figure 4.4. All of them have 3 mm long pins, which are based on the cylindrical one (C) and had an M4 right hand thread incorporated before other features were manufactured.

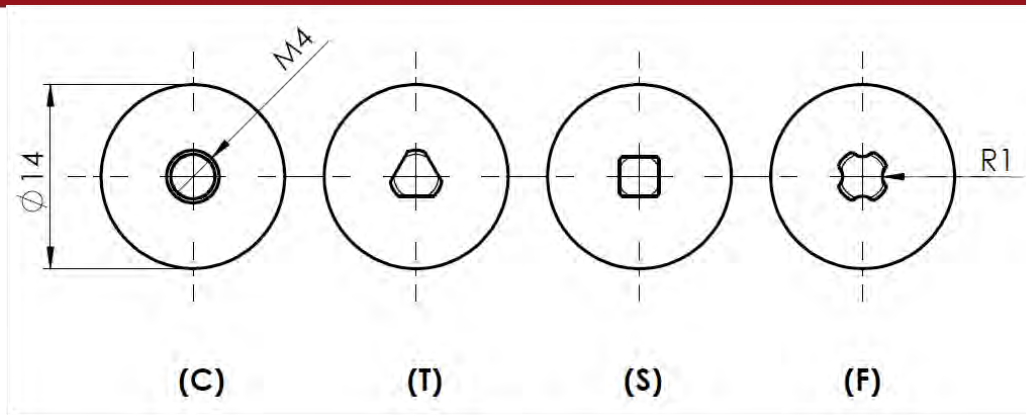


Figure 4.4: Tool geometries: (C)-cylindrical, (T)-triangular, (S)-square, (F)- cylindrical with flutes

4.3 Processing

Pretrials were carried out using the cylindrical and square profile, to find optimal parameters for the main trials. Therefore double-walled CNTs (DWCNTs) with a diameter of 5 nm and length ranging from 5 μm to 15 μm were used.



(a) Channel closing with a pinless tool



(b) FSP of the closed channel

Figure 4.5: Closing and processing of the CNT-filled channels

Before undergoing FSP, a pinless tool was used to seal the channels, using a plunging depth of 0.1 mm at 100 mm/min and 1500rpm as shown in figure 4.5a. This was done to avoid the powder being pushed out by the pin, as observed in the pretrials. The samples were then subjected to one pass FSP using different parameters and the four different tool geometries as shown in figure 4.5b. The direction of the tool rotation was always set counterclockwise

to provide a downward forge and vertical mixing as described in the literature. Therefore a Mazak VTC 16B CNC vertical machining center was used. The resulting 36 joints were named combining the abbreviations for the pin profile as shown in figure 4.4 and the parameter set number from table A.1. C4 for example stands for a joint produced by the cylindrical, threaded tool at 40 mm/min and 1600 rpm. A table with all the sample/parameter abbreviations can be found in the appendix.

Table 4.2: FSP parameters

No.	Rotational speed in rpm	Travel speed in mm/min	Feed rate in rev/min
1	20	1600	0.0125
2	20	1800	0.011
3	20	2000	0.01
4	40	1600	0.025
5	40	1800	0.022
6	40	2000	0.02
7	60	1600	0.375
8	60	1800	0.033
9	60	2000	0.03

4.4 Sample characterisation

After processing, plan views were taken from each joint using a Leica S6D stereo microscope. After that, different pieces were cut out of the plates to perform metallography and other examinations as illustrated in figure 4.6. Therefore a manual cutting machine, model Struers Labotom-3, with a cut-off wheel, model Buehler MetAbrase, was used. The cut out pieces were mounted into metallography mounts with a diameter of 30 mm using a Buehler SimpliMet mounting press and Buehler TransOptic powder (thermoplastic acrylic). Manual grinding of the resultant samples was carried out from P400 to P1200 followed by manual polishing using 3 μm , 1 μm and 0.3 μm polishing cloths, Buehler MetaDi 3 μm diamond paste and MicroPolish alumina suspensions with the respective particle sizes.

The polished samples were then etched with 0.5 % HF and pictures of the cross and longitudinal sections were taken with a Leica DMI5000 M microscope. The maximum size of the nugget and flow arm were measured for every cross section like in figure 4.7. Furthermore the electric resistance was measured on the 40 mm long samples, which had been cut out from the nugget area as shown in 4.6. A digital micro-ohmmeter MPK253 with a resolution of 1 $\mu\Omega$ at 10 A and

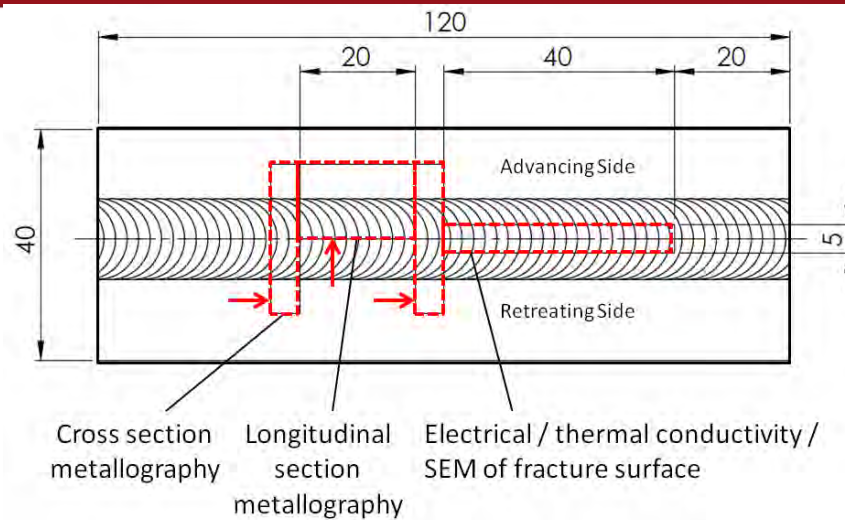


Figure 4.6: Sample geometry

a basic accuracy of 0.2% was used. In order to obtain a further resistance decrease, the samples were annealed at 400 °C for 3 hours and then measured again.

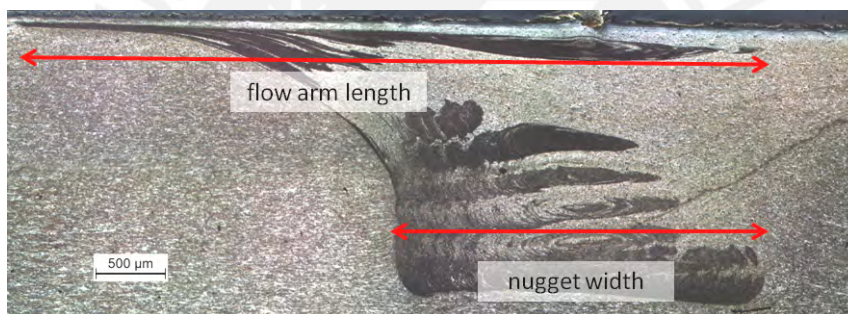


Figure 4.7: Measure points for nugget and flow arm width

The polished cross sections were also subjected to microhardness measurements on a Vickers hardness tester Zwick ZHV30 with a testing load of 200 g to distinguish areas with CNTs incorporated and areas, where the strong plastic deformation led to similar etching behaviour. At last, SEM analysis was carried out on a few selected samples on a FEI QUANTA 200 SEM to evaluate CNT agglomeration within the matrix and possible damage due to process forces. Possible tool wear was evaluated after processing by optical analysis using the Leica S6D stereo microscope.

5 Results

5.1 Plan views

Plan views of every joint were taken to provide a first impression about the joint quality. Figure 5.1 shows joints produced by the four tools with a parameter set with relatively low feed rates. As can be seen, the cylindrical tool produced a smoother surface than the other profiles but a slight surface lack of fill was encountered, which is an indicator for a excessively hot joint. The other joints in this figure show signs of surface galling, which is also caused by a too hot joint. The resulting feed rates were selected this low, because the cylindrical profile produced surface cracking at higher feed rates in the pretrials. Regarding the rest of the maintrial plan views at varying parameters, it could be summarized that the triangular and square profile generally produced relatively smooth surface while the fluted profile led to excessive surface galling.

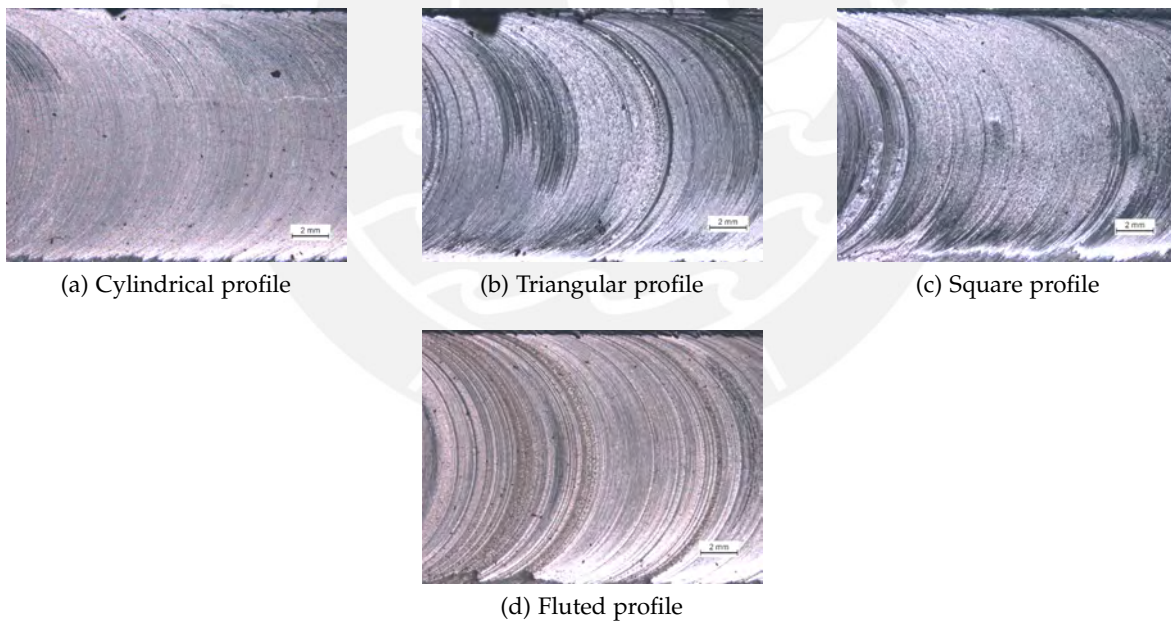


Figure 5.1: Plan views of joints produced at 1800 rpm and 20 mm/min with the different tool profiles

Furthermore one channel was processed with the same parameter set like the sample in figure 5.1d, but without CNTs. Figure 5.2 shows a plan view of this joint, that exhibits excessive surface lack of fill.

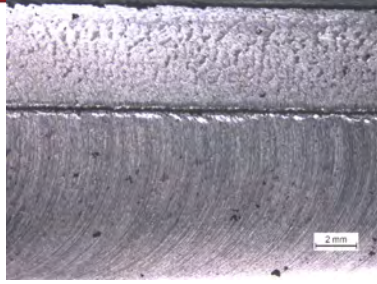


Figure 5.2: Plan views of an F2 (1800 rpm; 20 mm/min) joint without CNTs incorporated

5.2 Metallography

Two cross sections were cut out of each joint and prepared metallographically as described in section 4. The analysis of the pictures revealed different flow patterns for the different tool profiles. The cylindrical and square profile were used in the pretrials to find an optimal set of parameters to evaluate the tools over different feed rates. As the resultant feed rates led to the formation of wormhole defects, which is an indicator for too high travel speeds, in almost all the samples, the process limits were adjusted to introduce more heat into the joints.

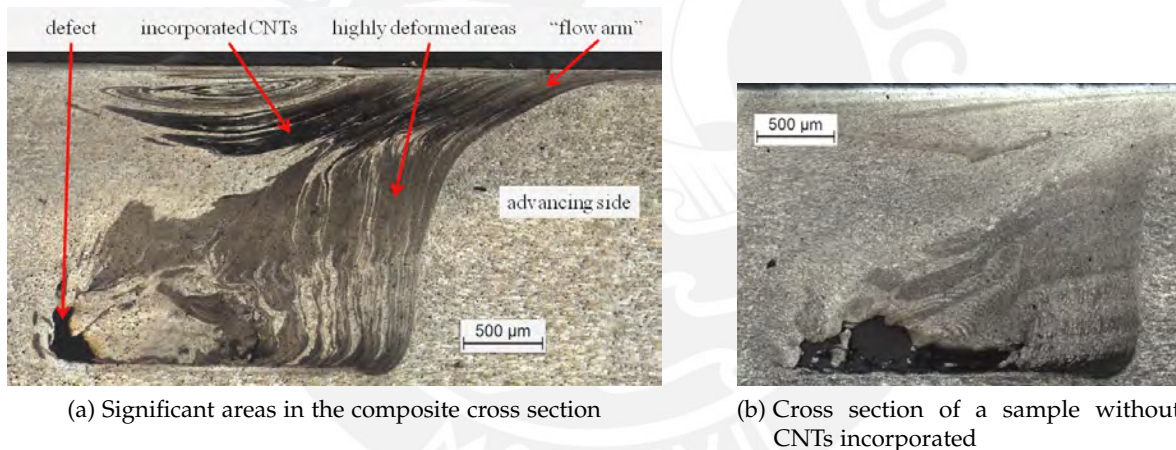
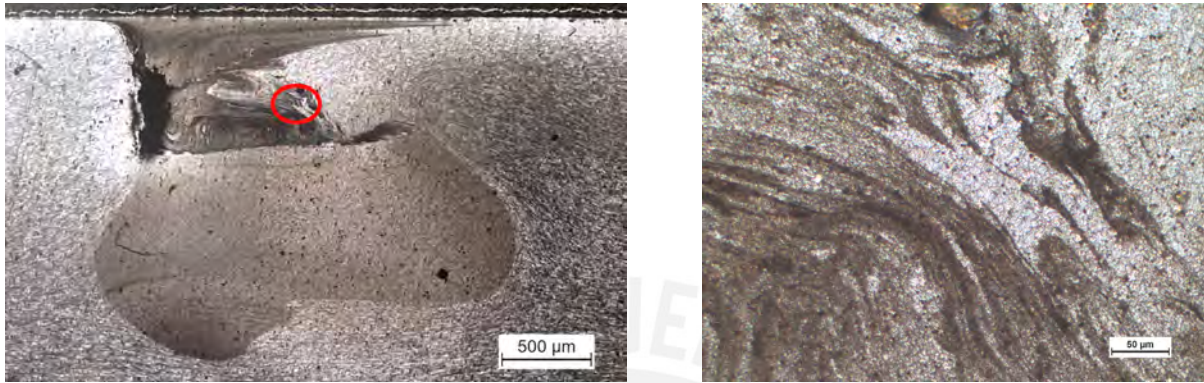


Figure 5.3: Metallographic analysis of the cross sections

For a better understanding, figure 5.3 shows an example of a cross section with the significant areas marked. Areas, where CNTs are actually incorporated, show a very dark tone, which occurs due to micron grain forming around the CNTs and makes this area also appear larger than it is. The area in the bottom of the nugget usually shows a similar etching behaviour because of high deformation rates, but contains no CNTs. This can be verified by figure 5.3b, which was processed without prior channel filling. Furthermore, the nugget is never formed symmetrically. Due to the superposition of rotational and forward movement of the tool, a "flow arm" is formed on the advancing side and thus makes it possible to distinguish the sides. Regarding the longitudinal section, it is important to consider that it only gives a tendency

about the process stability as the nugget was not always caught exactly in the middle when cutting the samples.

5.2.1 Cylindrical profile



(a) Overview

(b) Detailed view

Figure 5.4: Cross section of sample C3 (2000 rpm; 20 mm/min)



(a) C1 (1600 rpm; 20 mm/min)

(b) C5 (1800 rpm; 40 mm/min)



(c) C6 (2000 rpm; 40 mm/min)

Figure 5.5: Cross sections of sample C1, C5 and C6

As shown in figure 5.4, the joints produced by the cylindrical pin still exhibited hole defects in most of the samples. The CNTs were generally found to be distributed within a small area above the nugget. In this area, lamellas were formed as shown in figure 5.4b and revealed a very fluctuating distribution of the CNT densities. The nugget itself always showed a distinct boundary to the TMAZ. Figure 5.5 shows three more samples, which were processed with the cylindrical, threaded tool. As can be seen, a hollow defect occurred inspite of the paramteter variation and thus indicates insufficient material flow. The formation of so called onion rings also occurred in the nuggets, which is caused by the interaction of shoulder driven and pin driven material according to Kumar and Kailas [KK08]. Furthermore, signs of nugget collapse were encountered at increasing rotational speeds and indicate a too hot joint.



Figure 5.6: Sheared metal particles in the defect of sample C4 (1600 rpm; 40 mm/min)

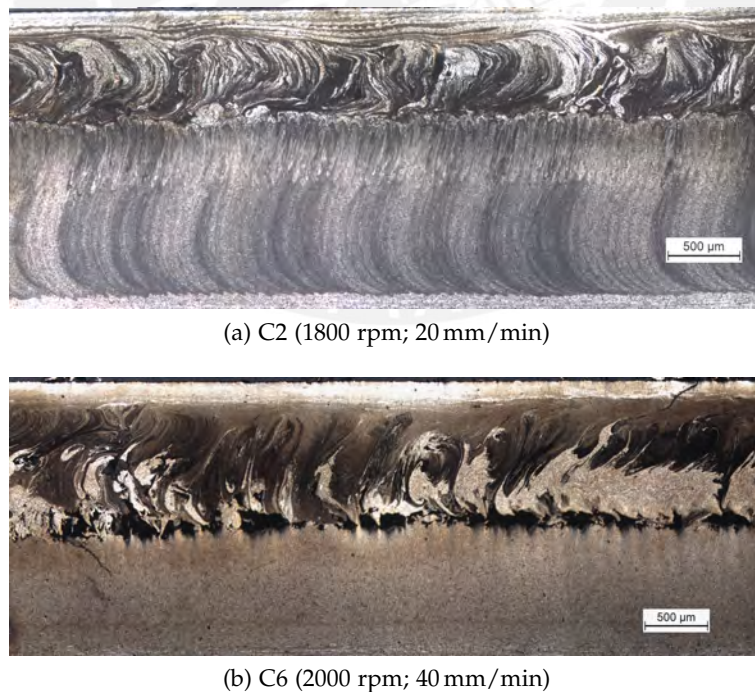


Figure 5.7: Longitudinal sections of sample C2, C5 and C6

At the same time, small pieces of barely plasticized material were found in some defects near the sections with CNTs as shown in figure 5.6. Also known as "chip lack of fill", these particles are sheared or cut off the parent material and deposited in the defect due to a too cold joint and insufficient material flow. The longitudinal sections of the joints produced by this tool also revealed the formation of defects and a very unsteady, almost periodic distribution of the CNT powder in the upper nugget area towards the processing direction as shown in figure 5.7. The bottom area of the nugget also shows the formation of layers with different deformation degrees as already seen in the cross sections. The defects usually occurred below the area, where CNTs were incorporated and were found to be more pronounced at higher travel speeds.

5.2.2 Triangular profile

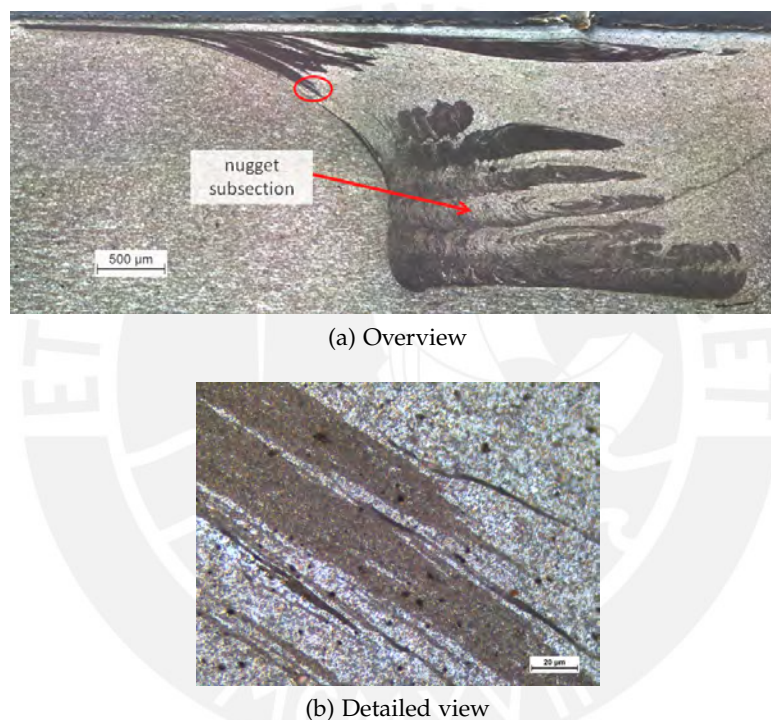


Figure 5.8: Cross section of sample T7 (1600 rpm; 60 mm/min)

The FSP tool with the triangular profile was the only tool, that produced defect-free joints almost over the whole parameter set. The CNT powder was always found to be dispersed in a wide area very close to the surface as shown in figure 5.8a. The nugget shows a rather rectangular shape. Furthermore it seems to be divided into 4 to 5 single nuggets, which are overlapping each other. The detailed view in figure 5.8b shows, that the CNTs are distributed in layers, which are almost parallel to each other. A vertical mixing effect can only be observed in areas on the advancing side, where the flow arm is formed. Figure 5.9 shows two more cross sections of joints produced by the triangular profile. Here it can be seen, that this profile led to relatively stable process without defect formation and also a fine distribution of the CNTs over



(a) T1 (1600 rpm; 20 mm/min)



(b) T3 (1800 rpm; 40 mm/min)

Figure 5.9: Cross sections of sample T1 and T3



(a) T3 (2000 rpm; 20 mm/min)



(b) T8 (1800 rpm; 60 mm/min)

Figure 5.10: Longitudinal sections of sample T3 and T8

a large area. The longitudinal sections of the joints in figure 5.10 also show, that a continuous flow pattern was produced and that the CNTs are dispersed uniformly along the processing direction. Almost all longitudinal flow patterns were formed as shown in figure 5.10a. Only at the highest travel speeds of the set, defects were formed as shown in figure 5.10b.

5.2.3 Square profile



(a) S1 (1600 rpm; 20 mm/min)



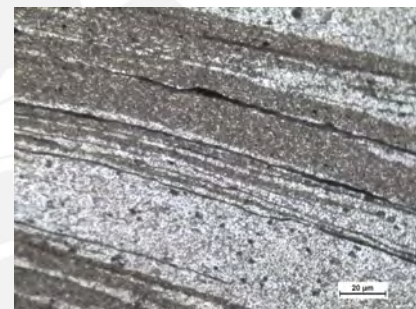
(b) S2 (1800 rpm; 40 mm/min)



(c) Detailed view of S2



(d) S6 (2000 rpm; 40 mm/min)



(e) Detailed view of S6

Figure 5.11: Cross sections of sample S1, S2 and S6

In contrast to the triangular pin, the square pin produced defects in almost all the samples as shown in figure 5.11. The defects at the bottom of the nugget can also be seen in the longitudinal sections in figure 5.12. They were found to be slightly increased with increasing travel speed. Furthermore, fissures could be encountered in the area above the nugget as shown in the cross section in figure 5.11c. Apart from the fissures, the CNTs were distributed uniformly along the processing direction like when the triangular profile was used.

The joints produced by the tool with the square profile exhibited similar flow pattern like those produced with the triangular profile. The CNT-powder was also dispersed close to the joint surface over an area about two times wider than the nugget as shown in figure 5.11d. Figure 5.11e shows a detailed view of the area where the powder is mixed with the matrix material. As can be seen, parallel layers are formed and the actual powder is distributed in line-like patterns



(a) S2 (1800 rpm; 20 mm/min)

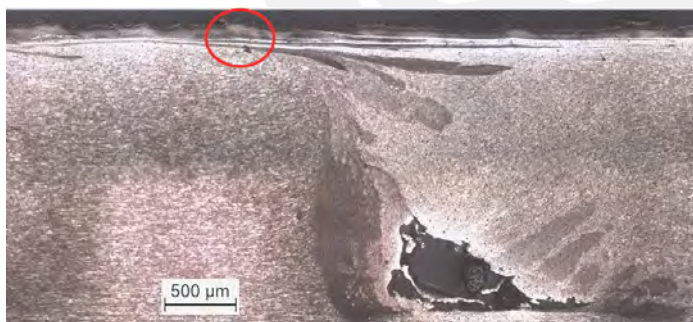


(b) S7 (1600 rpm; 60 mm/min)

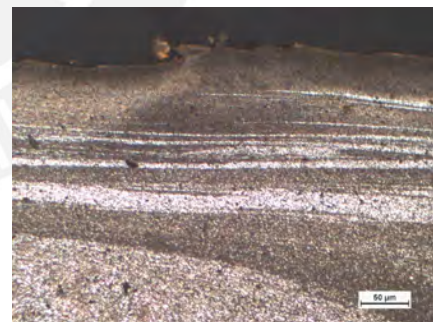
Figure 5.12: Longitudinal sections of sample S2, S4 and S7

but the area around also appears very dark due to the fine grain structure around those lines. The nugget was again found to be divided into some kind of subsections and very little vertical mixing occurred.

5.2.4 Fluted profile



(a) Overview



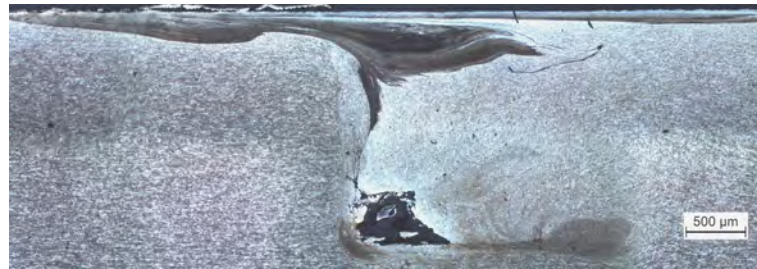
(b) Detailed view

Figure 5.13: Overview of sample F4 (1600 rpm; 40 mm/min)

The fluted profile was designed to provide an increased mixing effect by incorporating spherical undercuts. As it can be seen from the examples in figure 5.13 and 5.14, the CNTs were again distributed in layers and severe defect formation occurred in all the samples at the bottom of the nugget. On the other hand, an increased vertical mixing effect was obtained in comparison to the triangular and square profile. In general the nugget was again formed in a rather rectangular



(a) F7 (1600 rpm; 60 mm/min)



(b) F8 (1800 rpm; 60 mm/min)

Figure 5.14: Cross sections of sample F4, F7 and F8

shape and shows similarities to the other two profiles with "paddles". In the longitudinal sections in figure 5.15 the degree of the defect formation is more obvious. As shown, the tool produced continuous defects like channels. The CNTs were found to be dispersed more



(a) F2 (1800 rpm; 20 mm/min)



(b) F5 (1600 rpm; 60 mm/min)

Figure 5.15: Longitudinal sections of sample F2, F4 and F5

uniformly along the processing direction than when the cylindrical profile was used, but more irregularities than with the two previous profiles were encountered.

5.3 Flow arm and nugget size

As shown in figure 5.16, the profiles did not just produce different flow patterns, but also different nugget and flow arm sizes. The results are to be considered as tendencies as the nugget shape can vary along the processing direction. Regarding the nugget size, the cylindrical profile usually produced the widest nuggets, followed by the triangular profile. The square and fluted profile exhibited similar, but lower values. The results for the flow arm formation

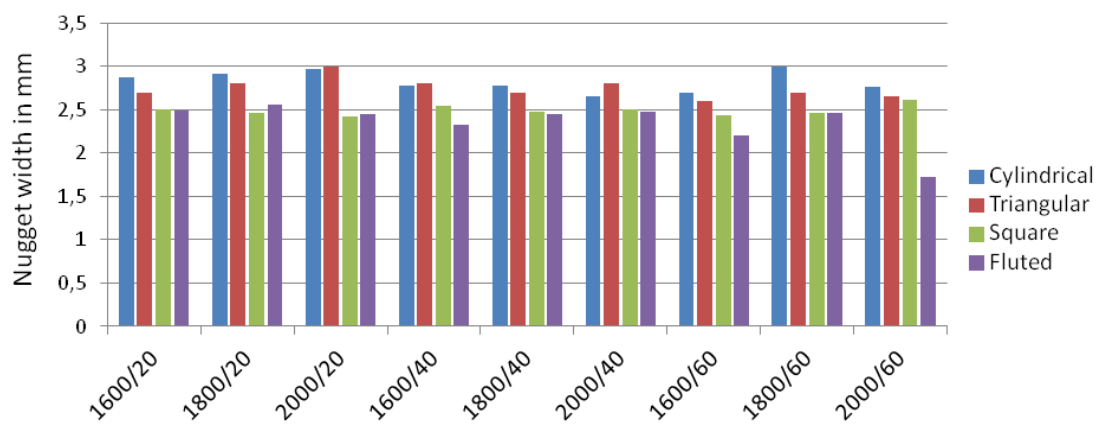


Figure 5.16: Nugget width at different parameter sets (caption: rotational speed/travel speed)

in figure 5.17 show more obvious differences. In most of the cases, the triangular and square pin produced the longest flow arms. In contrast to that, the fluted pin revealed up to 30% decreased values and the cylindrical pin revealed extremely low values, up to 70% below those of the triangular profile.

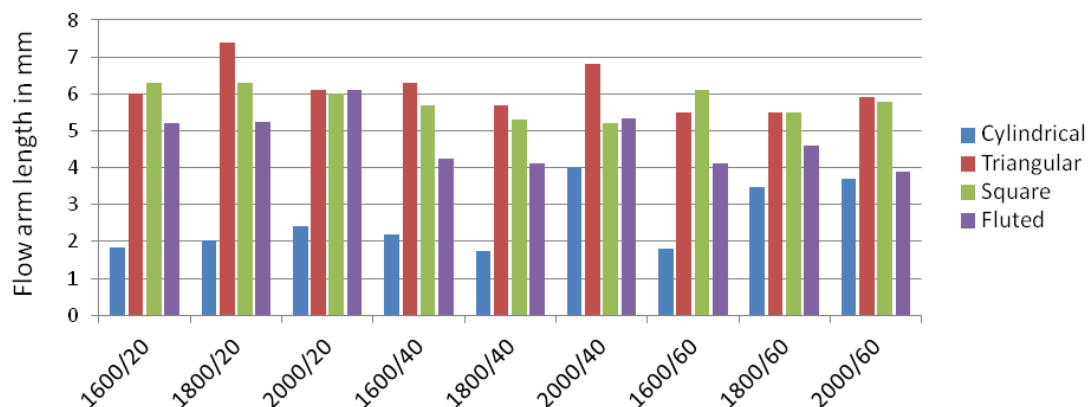


Figure 5.17: Flow arm length at different parameter sets (caption: rotational speed/travel speed)

5.4 Mircohardness measurements

Mircohardness measurement were carried out at various points within some selected cross section. Especially the areas, where CNTs were suspected to be incorporated, were points of interest. The hardness of the base material within the cross section lies between 64 HV and 70 HV. Figure 5.18 shows the resultant Vickers hardness values in HV. As can be seen, the areas, which are etched very dark and are thus suspected to carry CNTs, show hardness values up to 118 HV. This means, that an hardness increase of over 70% was achieved. Furthermore, the different areas could be distinguished better by comparing the hardness values. The layers, where CNTs have been incorporated, show values between 85 HV and 118 HV while areas with similar etching behaviour at the bottom of the nugget exhibit values between 75 HV and 85 HV. In less deformed areas with an accordingly brighter appearance, values between 65HV and 75HV were measured.

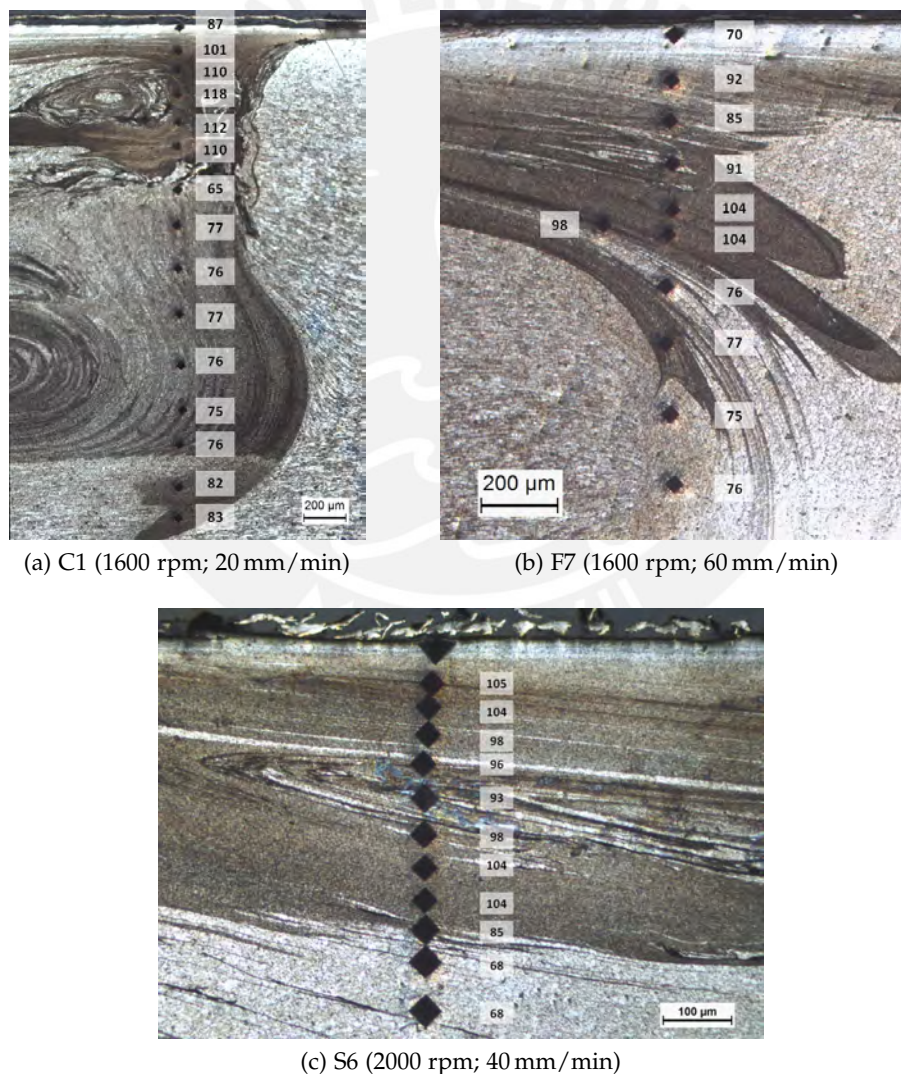


Figure 5.18: Mircohardness values (HV) in the cross sections of sample C1, F7 and S6

5.5 Electrical resistance

The pretrials were carried out using different combinations of travel speed, feed rate and tool profile to set up a frame for the maintrials. The measured resistances are shown in figure 5.19. No obvious correlation between the values and tool profiles or parameters could be obtained. Three samples were annealed at 400 °C for 2 hours after processing and a decrease of about 10% was achieved, but still above the base material. The sample, which was fabricated without CNTs using the tool with the square profile, showed the highest resistance but also a big, continuous defect at the bottom of the nugget. The electrical resistance of the resulting 36 samples was also measured as described in chapter 4. The values of the specific electrical resistances are shown in figure 5.20 with the mentioned sample abbreviations and B for base material. As can be seen, there is no significant correlation between the different values. The heat treatment, which was performed to decrease the resistance by eliminating the fine grain structure, did not show an effect either.

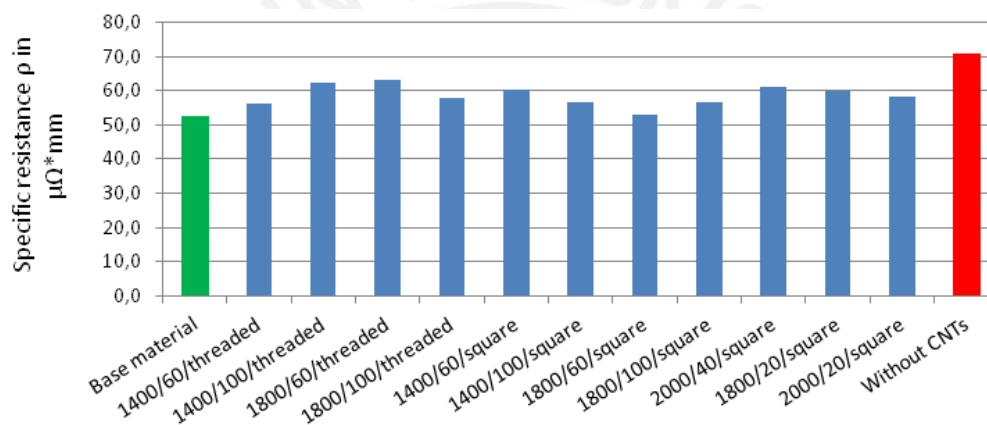


Figure 5.19: Specific electrical resistance of the pretrial samples after FSP, sample indication: rotational speed/ travel speed/ tool profile

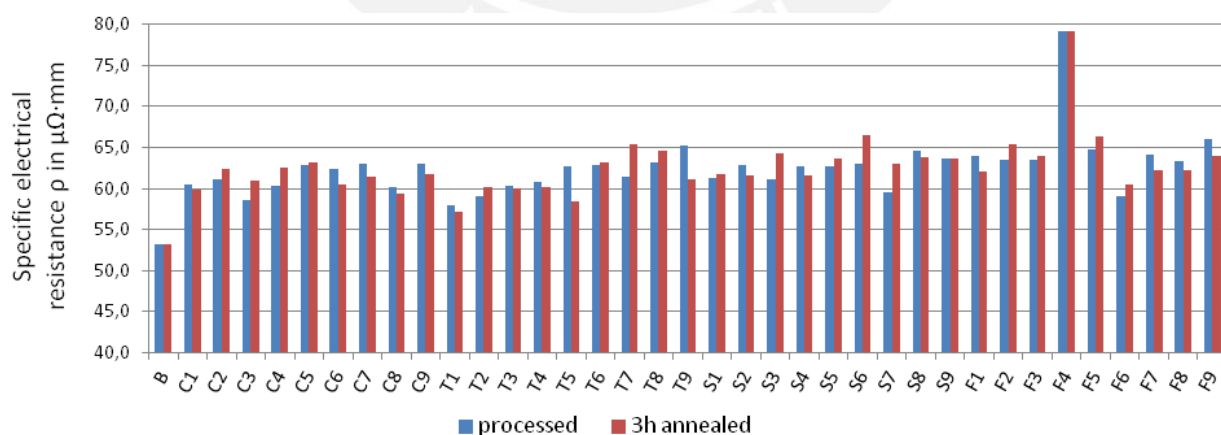
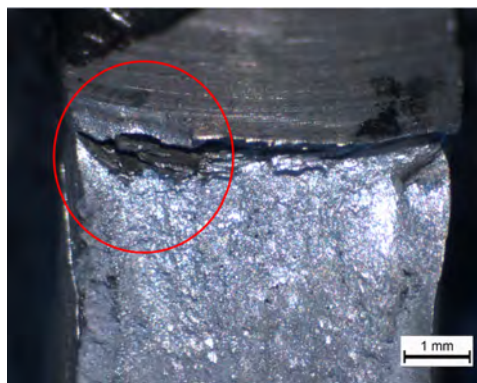


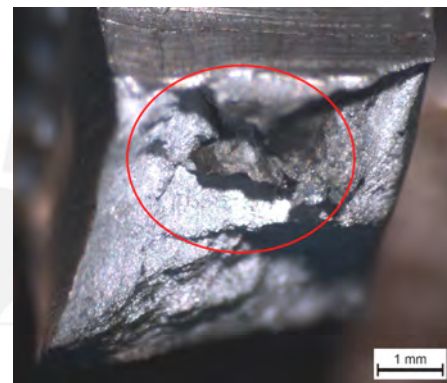
Figure 5.20: Specific electrical resistance of the samples after FSP and 3 hours annealing at 400 °C

5.6 SEM analysis

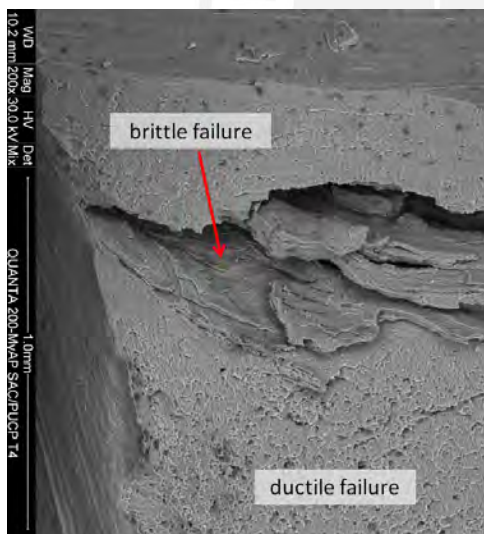
The SEM analysis of the fracture surfaces of a few, selected samples revealed different material failure behaviours within the processed section. Figure 5.21 shows a view of the fracture surfaces of sample T4 and C5. As can be seen, the material below the area with incorporated CNTs in figure 5.21c shows ductile failure behaviour while the CNT-reinforced layers in the upper part show brittle fracture properties and were separated from the lower part during tensile testing. Furthermore the reinforced area shows darkening within the layers, which appear like shadows and indicate the presence of lightweight elements like carbon.



(a) Optical microscope image of T4



(b) Optical microscope image of C5



(c) SEM image of T4



(d) SEM image of C5

Figure 5.21: Optical microscope and SEM image of the fracture surfaces of T4 and C5

In order to visualize the distribution of the CNTs within the fracture surface, a SEM spectroscopy mapping was carried out in this area. The results are illustrated in figure 5.22. As can be seen, the CNTs are distributed well, but higher concentrations can be found within the fissures as already seen in prior investigations. The areas with higher concentrations were therefore

analysed with higher resolution and single CNTs were found to be incorporated into the aluminium matrix as shown in figure 5.23.

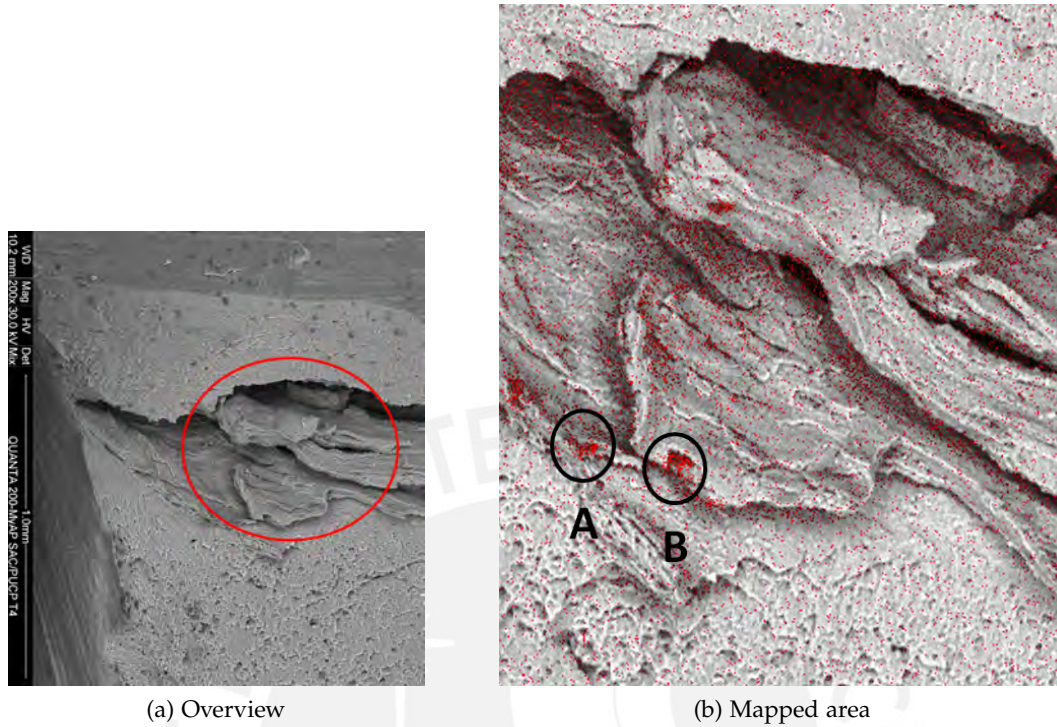


Figure 5.22: SEM mapping of the fracture surface, indicating carbon

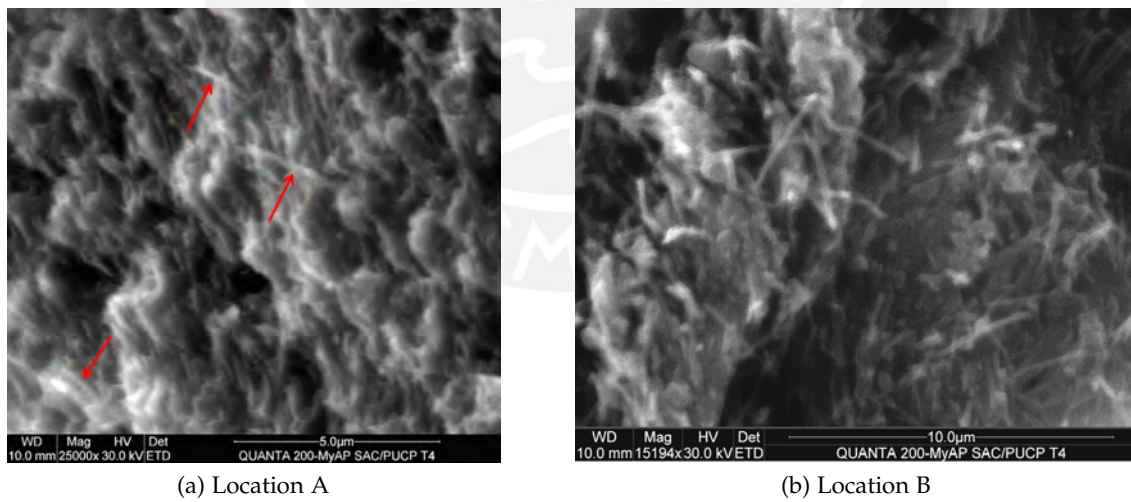


Figure 5.23: CNT incorporated into the Al matrix

5.7 Tool wear

The tools were examined under the stereo microscope after the main trials. The triangular and fluted profile had been operating 33 min in total, the cylindrical and square one slightly more due to the pretrials. As expected, no signs of excessive wear could be encountered but the plasticised aluminum was found to be sticking between the thread flanks as shown in figure 5.24. It can be assumed that the deposited material gets pushed out again in every trial due to the high process forces and temperatures.

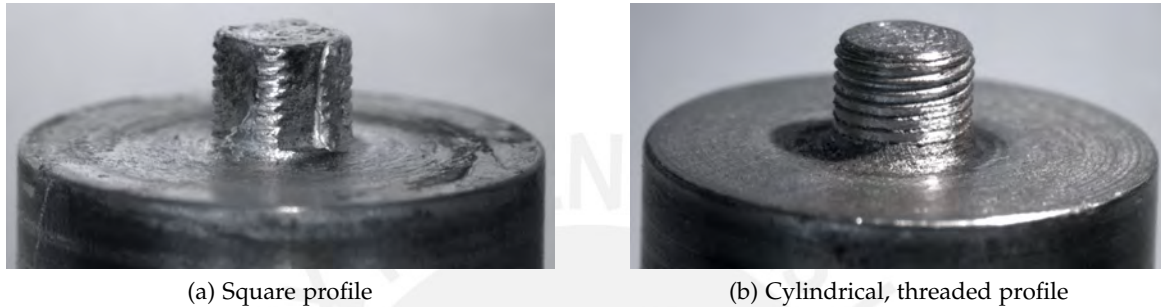






Figure 5.24: Deposited aluminum between the thread flanks of the tools

5.8 Summary

The metallographical analysis of the cross and longitudinal sections of the different samples revealed different flow patterns and CNT distributions for the four different tool profiles. Table 5.1 shows a ranking and summary of the results. The conventional tool with a cylindrical, threaded pin produced a classical shaped nugget with the CNTs dispersed in a small area above the nugget. Vertical mixing was found to be increased but the distribution of the CNTs was not stable along the processing direction. Furthermore, signs of nugget collapse were encountered at high rotational speeds. This means that both too high and too low heating was indicated by the occurred defects.

The tools with the triangular and square profile showed the best result regarding process stability and distribution as shown in figure 5.25, though the square profile produced defects at the bottom of the nugget. The CNTs were always dispersed over a wide area close to the joint surface and stretching up to the retreating side, especially at low travel speed. The nugget was always found to be in a rather rectangular shape and divided into subsections. As shown in figure 5.25a, the fluted tool revealed less favourable properties by producing a continuous defect in all the samples. Apart from this it showed similar flow pattern like the triangular and square profile. It also distributed the CNTs over a wide area but never up to the retreating side.

Table 5.1: Summary of the results

Ranking	Tool pin profile	Cross section	Properties
1	Triangular		<ul style="list-style-type: none"> - CNTs distributed uniformly over a wide area, - long flow arm, wide nugget, - no defect formation (only at high travel speed), - stable CNT distribution in processing direction.
2	Square		<ul style="list-style-type: none"> - CNTs distributed uniformly over a wide area, - little defect formation in all joints, - relatively stable CNT distribution in processing direction.
3	Fluted		<ul style="list-style-type: none"> - CNTs distributed uniformly over a relatively wide area, but not up to the retreating side, - severe defect formation in all joints, - increased vertical flow compared to the triangular and square profile, - relatively stable CNT distribution in processing direction.
4	Cylindrical		<ul style="list-style-type: none"> - CNTs distributed within small area above the nugget, - defect formation and insufficient material flow in all joints, - unstable CNT distribution in processing direction.

By measuring the microhardness in the cross sections, it was possible to distinguish regions with incorporated CNTs and regions with increased deformation (like at the bottom of the nugget). Both showed similar etching behaviour but the areas with CNTs revealed over 70% increased values compared to the base material while the "normally" deformed areas only showed increases up to 32%.

The electrical measurements revealed no significant correlation between tool geometry and specific electrical resistance, though the samples of the pretrials showed lower resistances than not reinforced samples. At the same the pretrial samples exhibited a resistance decrease of about 10 percent after annealing at 400 °C, but a lower resistance than that of the base material was not achieved.



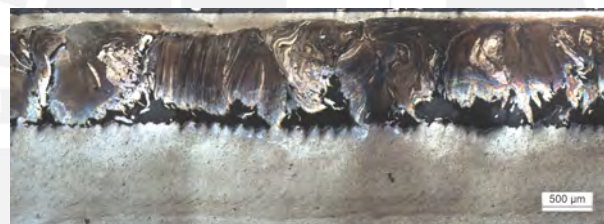
(a) T5



(b) S5



(c) F5



(d) C5

Figure 5.25: Longitudinal sections of the joints produced by different tool profiles at parameter set 5 (1800 rpm; 40 mm/min)

By SEM analysis the distribution of the CNTs could be evaluated at higher resolution than possible with the optical microscopy. Single CNTs were found to be incorporated into the Al matrix and in some areas agglomerated within fissures, but thus survived the high process forces. The SEM mapping of carbon shown a good distribution of the CNTs in the reinforced area. Furthermore the reinforced part of the fracture surface showed shearing of layers and rather brittle failure behaviour while the parent material showed ductile fracture properties.

6 Discussion

6.1 Material flow

As illustrated in chapter 5, the different tool profiles revealed different flow patterns and distributions of the CNTs within the metal matrix. The triangular profile showed the best performance over the whole parameter sets and distributed the CNTs close to the sample surface. Similar flow patterns were produced by the square profile. It can be concluded, that the surface-near distribution of the CNTs is caused by the fact, that relatively little thread was left on these pin profiles. Thus, the vertical mixing is very limited, which also explains the separation of the nugget into subsections. In this case the fluted pin represents an interstage between increased and no vertical mixing as the nugget gets separated but the subsections are drawn to the upper area on the retreating side.

As microhardness and SEM analysis revealed, a strong hardness increase is caused by the incorporated CNTs. This also leads to a separation of the reinforced zone from the base material during tensile testing as different failure behaviours occur. Due to the fact, that layers had been sheared of within the rather brittle area, it can be assumed, that the CNTs were dispersed very fine but still in form of lamellas. This is also verified by the SEM mapping results and the hardness values in this area, which are strongly increased but still vary between about 85 HV and 118 HV.

Comparing the measured sizes of the CNT-reinforced area, it can be seen, that the triangular profile produced the widest flow arm, as the CNTs were also dispersed over to the retreating side. This side usually exhibits poor material flow, as rotation and travel direction of the tool are opposite in this area and the material is only extruded around the pin but does not actually rotate with it. It is therefore concluded, that the triangular profile exhibits an enhanced material flow and produces turbulences and material suction due to the pulsating stirring caused by the flanks. Figure 6.1 shows a theory about the formation of suctions (disregarding the travel direction) caused by the tool geometries with flanks or undercuts.

It is assumed, that the triangular pin produces stronger suction and hence provides more material for filling the channel cavity for two reasons:

- The distance between the outer and inner diameter of the profile (\approx flank length) is longer, thus more underpressure is produced.

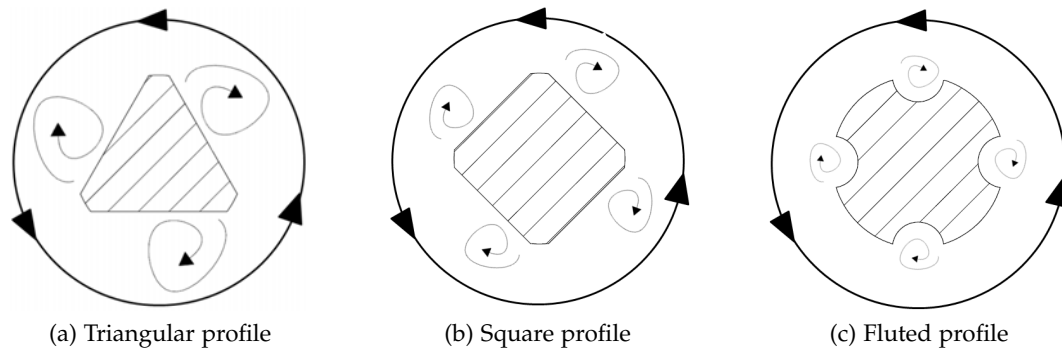


Figure 6.1: Turbulence/suction formation with different tool profiles

- The time between two "pulses" is longer and enables the inert, plasticized material to be "sucked in" and fill the cavity.

The cavity at the bottom of the nugget is assumed to be formed, when the channel surface is closed by the shoulder driven material flow and the pin driven material flow does not provide enough material from the sides to close this cavity completely. This theory can be confirmed by the fact, that the tool with the triangular pin produces a wide nugget and an extreme long flow arm below the tool shoulder, where the material is plasticized well by the friction with the shoulder and can be pulled into the nugget area more easily. Hence no defects occur, because the additional material fills the cavity. The square profile produces similar flow patterns but due to the lower flank length, less underpressure and turbulence is produced. Furthermore the time between two pulses is shorter and the material flow is not enhanced sufficiently. Nevertheless only small defects and wide CNT-reinforced areas are produced.

As shown in figure 6.1c, the fluted pin only produces very small turbulences within the flutes, which is not enough to fill the cavity but produces similar flow patterns like the two other profiles. The cylindrical pin produces an enhanced material flow within the thread flanks and hence provides vertical mixing, which leads to the high values in nugget width. On the other hand the material, which is drawn down by the threads, is missing on the top to fill the channel and cannot be compensated from the sides. Consequently, the defect occurs in the upper section of the nugget.

6.2 Heat flow

As illustrated before, the cross sections of joints produced by the cylindrical tool revealed defects caused by a too cold joint, like deposited metal chips in the hole defects. At the same time they showed signs of nugget collapse at higher rotational speeds, which indicate a too hot joint. An explanation for the occurrence of those defects in the same sample is, that a different temperature distribution was presumably caused by the incorporation of the CNTs. Due to

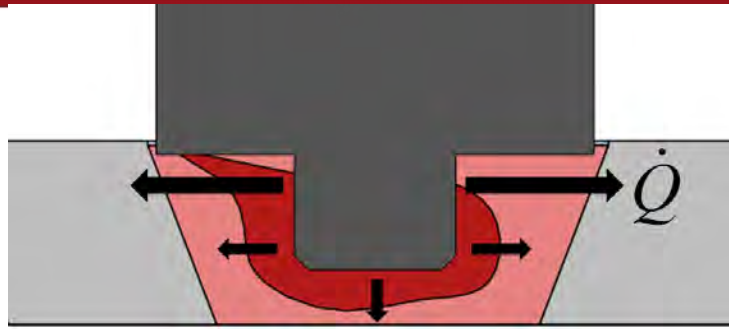


Figure 6.2: Schematic heat flow in the processed section

their extreme high thermal conductivity the frictional heat in the upper section of the joint is transported faster to the sides and into the base material as illustrated schematically in figure 6.2. Thus the material is not softened enough to be mixed homogeneously and the formation of defects and fissures (as seen with the square profile) occurs. The high thermal conductivity of the CNTs also leads to the dark appearance of the sections, where CNTs had been incorporated. In these sections, heat conduction is increased, grain growth avoided and the resultant micron grain sizes cause the typical etching behaviour, which makes it difficult to distinguish parent material and CNT layers.

6.3 Electrical resistance

The electrical resistance measurements showed no significant decrease for CNT-reinforced samples and the resultant values always stayed above the resistance of the unprocessed base material. This is caused by the fact, that the electrical resistance is a quite sensitive indicator and is strongly influenced by defects and changes in microstructure. Especially the fine grain microstructure, which results from the high deformation degree during FSP, affects it severely. The deformation causes dislocations, dynamic recrystallisation processes and consequently an increased amount of grain boundaries, which represent barriers for the electron flow. In summary, the following factors interact with each other and lead to high resistance values in spite of the CNT reinforcement:

- fine grain microstructure,
- defect and fissure formation,
- agglomeration of CNTs in some areas, thus little attachment to the matrix,
- forming of low conductive carbide / oxide or metallic interphases during annealing,
- varying direction of the process forces due to the complex material flow,
- different CNT distribution patterns ↔ sample geometry (See section 6.4).

Because of that complex interaction, the influence of the CNT reinforcement cannot be analysed separately. For a better separation of the effects, a more controllable process with a less complex and more directed material flow is required.

6.4 Error consideration

6.4.1 Process

As the resultant formation of the composite is not only affected by the tool geometries and chosen parameters, but also by the process itself, some other factors have to be considered, which may have led to variations within the results. First of all, the channels were filled manually. Even though this was carried out as uniformly as possible, the volume fraction is assumed to vary. Furthermore the touching of the reference point was also carried out manually, which causes variations of the plunging depth. This parameter is also influenced by frictional heating as the tool is elongated by thermal expansion and the tool shoulder plunges in slightly deeper at the end of the joint. Consequently, more powder gets pushed out of the joint by the tool shoulder and the volume fraction decreases at this location. For the analysis of material flow patterns, these errors are not considered as critical but they certainly affect the resistance values in a way, that they can practically all be put into one stray area.

6.4.2 Sample preparation

The sample preparation also influences the reliability of the results. Especially the electrical resistance is affected again. The resistance sample width of 5 mm was selected, after pretrials with the cylindrical and square tool were carried out. With other tool profiles and enhanced processing parameters, much longer flow arms with CNTs incorporated were produced in the maintrials. Thus, some of the CNT reinforced areas were shortened during sample cutting. Together with the errors caused by the process, the CNT volume fraction can consequently not be assumed as uniform, which makes it hard to draw reliable conclusions from the resistance values. Furthermore the longitudinal sections were not always caught exactly in the middle of the nugget during cutting, which led to slight differences between the samples. Another deviation caused by the preparation method is, that the etching behaviour was not absolutely uniform for all the samples and caused varying contrasts or exaggerated certain parts of the joint.

7 Summary

In summary it can be concluded, that the geometry plays an important role for the material flow during FSP. While the vertical mixing effect of cylindrical, threaded tools might be favourable for processing abutting or overlapping plates, it is not suitable for closing a powder-filled channel or fabricating a surface composite. To obtain the desirable results, FSP and FSW have to be treated separately regarding the selection of tool geometries. In order to achieve a uniform particle distribution during composite fabrication, an enhanced horizontal material flow is required. Therefore, tools with flanks or undercuts, which provide partly turbulent material flow around the pin, are to be preferred. On the other hand, the limits of flank size and number have to be investigated further, as vortex breakdown can also cause defects at high rotational speed. The properties of the CNTs also have to be considered for the material flow, as their high thermal conductivity and reinforcing mechanisms change the heat and hardness distribution during the process, thus producing cracks and defects.

Regarding FSP for fabricating CNT-reinforced aluminum composites, the process was found to be a suitable method for incorporating CNTs in less process steps than with the powder metallurgy route. A relatively uniform distribution of the CNTs along the processing surface was achieved, which provides possible application for surface composites. In order to enhance electrical properties, the process revealed too many influences, that would inhibit an increase in conductivity, but further trials with an adjusted tool and sample geometry have to be carried out. Besides, it has to be investigated, if a uniform distribution within the matrix will necessarily affect the electrical conductivity. In general, forming processes show great potential to provide a good dispersion of the CNTs within the matrix as the prevention of liquid phase and high process forces counteract their agglomeration tendency.

8 Outlook

Some interesting conclusions could be derived from the material flow patterns and CNT-distribution in the different joints. They show, that the damage of the tubular CNT-structure through multi-pass FSP can be avoided by adjusting the tool geometry. Further investigations have to be carried out in order to verify the drawn conclusions and establish further theories on the behaviour of CNTs and material flow mechanisms during FSP.

Table 8.1 gives an overview over recommended subjects for further investigations.

Table 8.1: Recommendations for further investigations

Process section	Recommended investigation subjects
Tool geometry	<ul style="list-style-type: none"> - effect of other, more complex pin geometries - influence of relative size of pin and channel on defect formation - correlation between flank size / number (triangular, square, polygon) and nugget size - effect of different shoulder shapes (conical, with flutes and other features) - pin geometry limits regarding vortex breakdown
Process and samples	<ul style="list-style-type: none"> - variation of the channel cross section - method for ensuring a certain CNT volume fraction in the channel - variation of the shoulder plunging depth and tilt angle
Analysis	<ul style="list-style-type: none"> - analysis of the interphase of CNTs and matrix - correlation between CNT distribution, grain size and thermal/-electrical conductivity - influence of annealing on composite microstructure and conductivity - wear behaviour of the CNT-reinforced surface

At first, a different channel preparation method has to be developed to guarantee a stable volume fraction. Furthermore the correlation between relative size of pin and channel and defect formation has to be analysed. In general the influence of the pin and also shoulder profile has to be investigated further. Especially the effect of other, more complex pin and shoulder geometries has to be investigated as suggested in the literature. Therefore the process has to be adjusted in a way, that stable conditions and comparable results can be ensured.

Further analysis on the influence of annealing and interphase formation on the electrical and thermal conductivity has to be carried out as well. In order to that, the correlation between CNT

distribution and resultant grain size must be considered. The results of such investigations shall finally clarify the complex mechanisms during CNT-reinforced MMC fabrication and thus advance them on the route towards application.

